



Deposited via The University of Leeds.

White Rose Research Online URL for this paper:

<https://eprints.whiterose.ac.uk/id/eprint/136713/>

Version: Accepted Version

Article:

Colombera, L, Mountney, NP, Medici, G et al. (2019) The geometry of fluvial channel bodies: Empirical characterization and implications for object-based models of the subsurface. AAPG Bulletin, 103 (4). pp. 905-929. ISSN: 0149-1423

<https://doi.org/10.1306/10031817417>

Copyright © 2019. The American Association of Petroleum Geologists. All rights reserved. This is an author produced version of a paper published in AAPG Bulletin. Uploaded in accordance with the publisher's self-archiving policy.

Reuse

Items deposited in White Rose Research Online are protected by copyright, with all rights reserved unless indicated otherwise. They may be downloaded and/or printed for private study, or other acts as permitted by national copyright laws. The publisher or other rights holders may allow further reproduction and re-use of the full text version. This is indicated by the licence information on the White Rose Research Online record for the item.

Takedown

If you consider content in White Rose Research Online to be in breach of UK law, please notify us by emailing eprints@whiterose.ac.uk including the URL of the record and the reason for the withdrawal request.

The geometry of fluvial channel bodies: Empirical characterization and implications for object-based models of the subsurface

Luca Colombera*, Nigel P. Mountney, Giacomo Medici, L. Jared West

School of Earth & Environment, University of Leeds, LS2 9JT, Leeds, UK

*) corresponding author: l.colombera@leeds.ac.uk

Abstract

The distribution of channel deposits in fluvial reservoirs is commonly modeled with object-based techniques, constrained on quantities describing the geometries of channel bodies. To ensure plausible simulations, it is common to define inputs to these models by referring to geologic analogs. Given their ability to reproduce complex geometries and to draw upon the analog experience, object-based models are considered inherently realistic. Yet, this perceived realism has not hitherto been tested by assessing the outputs of these techniques against sedimentary architectures in the stratigraphic record.

This work presents a synthesis of data on the geometry of channel bodies, derived from a sedimentologic database, with the following aims: (i) to provide tools for constraining stochastic models of fluvial reservoirs in data-poor situations; (ii) to test the intrinsic realism of object-based modeling algorithms by comparing characteristics of the modeled architectures against analogs.

An empirical characterization of the geometry of fluvial channel bodies is undertaken that describes distributions in, and relationships between, channel-body thickness, cross-stream width, and planform wavelength and amplitude. Object-based models are then built running simulations conditioned on six alternative analog-informed parameter sets, using four algorithms according to nine different approaches. Closeness of match between analogs and models is then determined on a statistical basis.

Results indicate which modeling approaches return architectures that more closely resemble the organization of fluvial depositional systems known from nature, and in what respect. None of the tested algorithms fully reproduce characteristics seen in

natural systems, demonstrating the need for subsurface-modeling methods to better incorporate geologic knowledge.

Keywords: fluvial architecture; channel; alluvial aquifer; fluvial reservoir; reservoir model; aquifer model.

1. Introduction

Because the accumulated deposits of alluvial depositional systems are heterogeneous at multiple scales, geologic analogs comprising well-exposed outcrop successions are extensively used to understand and predict heterogeneity in the sedimentary architecture of alluvial aquifers (e.g., Biteman et al., 2004; Klise et al., 2009; Höyng et al., 2014; Piro et al., 2015) and hydrocarbon reservoirs (e.g., Bridge et al., 2000; Dalrymple, 2001; Pranter et al., 2007; Fabuel-Perez et al., 2010). Channelized fluvial deposits representing channel fills, the aggradation of channel belts, or part or all of the infill of valleys, form the main components of most fluvial reservoirs and aquifers, because they typically contain the majority of the potentially producible volumes. Therefore, the distribution of channel and overbank deposits is tentatively reconstructed in workflows of subsurface characterization, a process aided by insight from outcrop studies of geologic analogs.

In subsurface studies, simulations of the distribution and geometry of channel deposits, and assessment of the related uncertainty, are commonly attempted by applying stochastic modeling techniques, which allow multiple equiprobable realizations of sedimentary architecture to be built. Object-based modeling algorithms constitute a category of such modeling methods. They operate by placing geologic bodies, treated as discrete objects, in the volume of interest, until a certain proportion or number of such objects is reached, while simultaneously ensuring that input parameters describing the geometry and topology of the objects and any conditioning data (e.g., well data) are honored, at least to certain tolerance thresholds (cf. Clemetsen et al., 1990; Gundesø and Egeland, 1990; Hirst et al., 1993; Holden et al., 1998; Viseur et al., 1998; Deutsch and Tran, 2002). Object-based algorithms can also be used to generate so-called training images, which are three- or two-dimensional geocellular grids employed as input to stochastic modeling methods based on multiple-point statistics (MPS). MPS methods use stochastic

pixel-based algorithms that derive conditional probabilities of occurrence of a category (e.g., sedimentary facies) in a certain position based on patterns borrowed from a training image and evaluated over multiple points (Guardiano and Srivastava, 1993; Strebelle, 2002). As applied to modeling the architecture of fluvial reservoirs or aquifers, training images are digital representations of sedimentary heterogeneity that, when intended to represent large-scale architecture, commonly incorporate sinuous channelized bodies in a background of overbank sediment (e.g., Strebelle, 2002; Feyen and Caers, 2006; Pyrcz et al., 2008; Eskandaridavand and Srinivasan, 2010; Gottschalk et al., 2017).

When utilizing object-based algorithms to model fluvial reservoirs, channelized objects are commonly chosen that represent discrete channel sandbodies. Object-based modeling methods require families of channel bodies to be parameterized by attributes describing their planform and cross-sectional geometries, in the form of distribution types and associated descriptive statistics. Thus, with these methods, data on the geometry of alluvial successions considered as appropriate analogs can be readily applied to subsurface predictions. However, a common problem is how to source suitable analog data that describe both the vertical and lateral extent, and the planform geometry of fluvial channel bodies. Additionally, even when this type of characterization can be undertaken, establishing analogy to a subsurface succession is not straightforward, and a base-case scenario grounded on geologic insight might therefore be desired.

The significance of selecting suitable analogs for defining the input to object-based models is highlighted by recognition of the impact of channel-body characteristics on the static and dynamic connectivity of fluvial reservoirs and aquifers (cf. McKenna and Smith, 2004; Larue and Friedmann, 2005; Larue and Hovadik, 2006; Hovadik and Larue, 2007; Liu and Atan, 2008; de Jager et al., 2009; Burns et al., 2010; Jha et al., 2016; Peter et al., 2017). Realistic reproduction of sandbody connectivity in fluvial aquifers and reservoirs is crucial to several applications, for example when predictions need to be made relating to the efficiency of hydrocarbon production, the behavior of contaminant plumes, spatial variability in groundwater drawdown, the viability of programs of carbon capture and storage, or optimal geothermal exploitation of hot sedimentary aquifers (e.g., Keogh et al., 2007; Ronayne et al., 2008; Giambastiani et al., 2012; Norden and Frykman, 2013; Issautier et al., 2014;

Jeong and Srinivasan, 2016; Nguyen et al., 2017; Willems et al., 2017; Marini et al., 2018). In this regard it is significant that object-based models are considered inherently realistic, thanks to their ability to reproduce complex predefined geometries and to leverage on analog data. In reality, this is merely a qualitative perception of realism, as a systematic quantified assessment of the outputs of these techniques against geometric attributes known and recorded from the geologic record has not hitherto been undertaken.

Thus, there are two outstanding problems associated with the construction of object-based models of channelized fluvial successions in the subsurface, which are addressed in this work: the need for constraints that are geologically sensible and applicable in data-poor contexts, and the unresolved uncertainty on the degree to which the products of object-based modeling algorithms are comparable to the stratigraphic organization of fluvial depositional systems known from nature. To these ends, the aim of this work is to present a synthesis of data on channel bodies derived from a large database that describes the sedimentary architecture of many fluvial successions, and to test whether commonly employed object-based geomodeling algorithms are appropriate as tools for subsurface characterization. The following specific research objectives are identified:

- (i) to provide empirical relationships that can be used for constraining object-based models of fluvial reservoirs and aquifers, particularly for cases where specific geologic analogs are not available;
- (ii) to test the intrinsic realism of four popular object-based modeling algorithms, by applying an analog dataset and comparing characteristics of the modeled architectures against fundamental patterns identified in the stratigraphic record.

After introducing the analog database and the tested modeling algorithms ('Materials and methods'), we present a synthesis of statistics on channel-body geometries from the studied analogs ('Characterization of geologic analogs'). We then demonstrate how this information can be applied to constrain object-based models for fluvial reservoirs, while presenting the design of the test chosen for assessment of the algorithms ('Object-based models: design of the test'). Subsequently, we compare the modeling outputs against the inputs, and more generally against the geologic

analog (‘Comparison between analogs and models’). Finally, we discuss the significance of the results for geologists and geomodelers who build object-based models of the subsurface, and for geostatisticians who develop object-based modeling algorithms (‘Discussion’).

2. Materials and methods

2.1 Analog data

Data on the architecture of fluvial channel bodies are obtained from the Fluvial Architecture Knowledge Transfer System (FAKTS), a database of sedimentologic datasets derived from the scientific literature and from original field studies (Colombera et al., 2012, 2013). FAKTS includes quantitative and qualitative data on sedimentary units belonging to three scales of observation: large-scale depositional elements; architectural elements (*sensu* Miall, 1985) and lithofacies. Depositional elements are large-scale sedimentary bodies classified as channel bodies (also termed ‘channel complexes’; Colombera et al., 2012) or floodplain elements on the basis of the interpreted origin of their deposits. The subdivision of stratigraphies in these units is partly based on geometric rules (cf. Colombera et al., 2012, 2013, 2015, 2016a).

As defined for FAKTS, a channel body represents a discrete sedimentary unit with channelized geometry and made of sediments deposited by one or more fluvial channels. Thus, a channel body does not possess a specific genetic or paleo-geomorphic significance: a channel body could therefore equally correspond to the preserved product of a channel belt, to an isolated channel fill, to a portion of valley fill, or to a compound amalgamated multi-story body. This generic categorization of channel bodies makes sedimentary units of this type widely applicable as objects employed in object-based modeling efforts that focus on large-scale fluvial architecture (e.g., Pranter et al., 2014).

The geometry of channel bodies stored in FAKTS is characterized in terms of morphometric parameters, four of which are used in this work (Figure 1): (i) the maximum thickness of the body; (ii) the maximum width of the body as measured orthogonally to its direction of elongation (i.e., along depositional strike); (iii) the

mean wavelength of any form of sinuosity that the body might display in plan-view, as averaged over the observed bends; (iv) the mean amplitude of sinuosity displayed in plan-view, as averaged over the observed bends. In this work, only true widths are reported: channel-body width data that relate to apparent measurements (i.e., as obtained along directions at an oblique angle with the axis of elongation of the channel body) and incomplete observations (e.g., because of outcrop termination) are excluded. Where channel bodies exhibit sinuous planforms that appear as having superimposed sinuosities, their planform is characterized in terms of mean amplitude and wavelength of the sinuosity that has the highest amplitude-to-wavelength ratio. Channel bodies are preserved deposits: their planform sinuosity does not necessarily – or even usually – equal the sinuosity of their formative river, though these quantities are related in some cases (cf. Stølum, 1998; Fryirs et al., 2016).

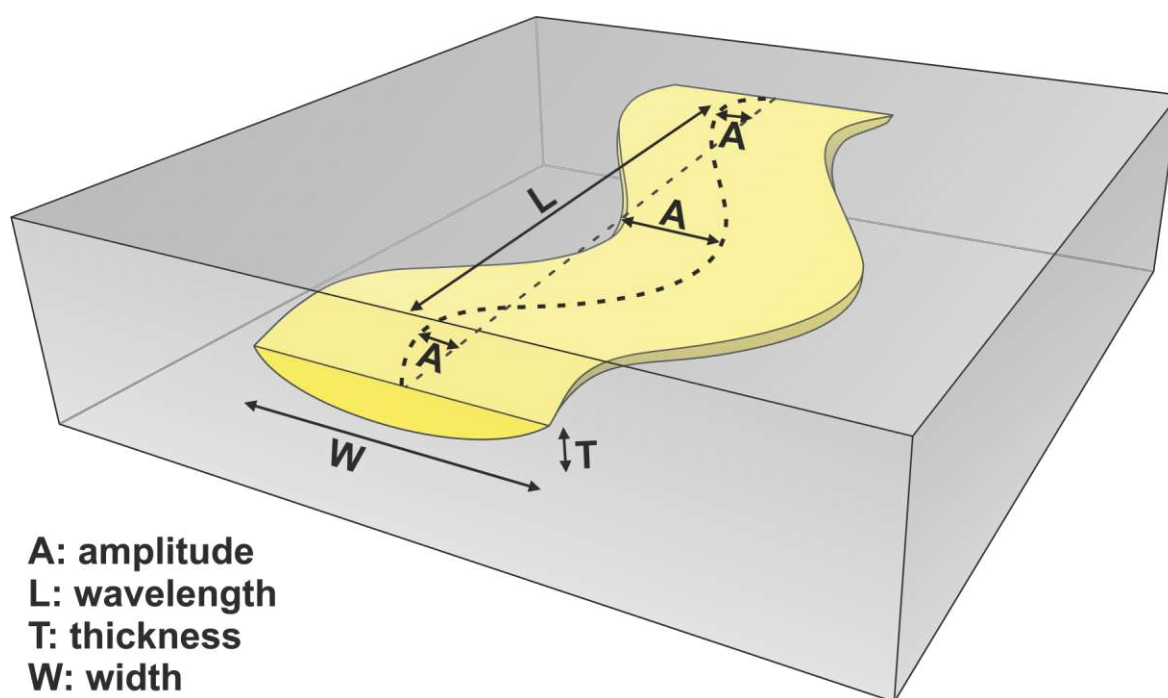


Figure 1: Morphometric parameters of FAKTS channel bodies. Note that channel-body amplitude is defined as half of the maximum displacement shown by the channel-body centreline along a complete wavelength, i.e., as in physics, and as opposed to how amplitude is sometimes defined in river descriptions (e.g., Leopold and Wolman, 1960; Williams, 1986) and in Schlumberger Petrel. The attributes shown characterize the geometry of preserved channelized sedimentary bodies, not the geometry of their formative river channels.

Data on channel-body geometries have been derived from studies that present datasets from outcrops (e.g., Kjemperud et al., 2008; Labourdette, 2011), three-

dimensional (3D) seismic surveys (e.g., Maynard and Murray, 2003; Alqahtani et al., 2015), and closely spaced cores in shallow deposits of Quaternary and modern systems (e.g., Jordan and Pryor, 1992; Berendsen and Stouthamer, 2001). Although the planform geometry of exhumed fluvial channel bodies can in some cases be seen in outcrop (e.g., McNally and Wilson, 1996; Williams et al., 2007), most of the data reported here on mean channel-body amplitude and wavelength are derived from subsurface datasets. The stratigraphies considered as analogs in this work are generally much larger than most channel bodies. However, any descriptive statistics of morphometric parameters suffer from volume support: larger samples provide more meaningful statistics, as they are more likely to capture the full extent of channel bodies and likely contain more units. For instance, smaller outcrops are less likely to display the entire width of the larger channel bodies, whose width would therefore be excluded from the analysis.

In FAKTS, analog case studies are arranged into subsets, which represent portions of datasets that are classified on attributes describing the depositional systems, their geologic controls, and related metadata. Each subset is effectively an analog sample, usually a stratigraphic volume. The data presented in this work relate to 6,476 channel bodies from 178 analog subsets. Data were taken from 59 literature sources, and complemented with data from two field studies whose results are now also published (Colombera et al., 2016b, 2017). The full list of literature sources is provided in the Supplementary material.

Data on the morphometric parameters that describe the architecture of channel bodies are used for (i) characterizing their statistical distribution in analogs and relationships that might exist between each of them, and (ii) compiling empirical equations that can be employed to predict descriptive statistics in any of these parameters from knowledge of others.

2.2 Modeling algorithms

The resulting characterization of channel-body architectures is also applied to test object-based modeling algorithms in terms of their ability to replicate the organization seen in the analogs.

Four popular algorithms for object-based modeling have been used in this test, to cover the range of ways in which models of this type can be constrained: FLUVSIM (publicly available; Deutsch and Tran, 2002), TiGenerator (publicly available; Maharaja, 2008), Tetris (publicly available; Boucher et al., 2010), and the algorithm implemented in Petrel 2014 (commercial software by Schlumberger). These codes are also used to build training images applicable to MPS modeling of fluvial successions (e.g., Pyrcz et al., 2008; Bezrukov and Davletova, 2010; Gottschalk et al., 2017).

Unconditional simulations (i.e., simulations that are not conditioned by hard or soft data, such as boreholes or seismic attributes) were run to generate 3D geocellular models of sedimentary architecture, consisting of channel bodies distributed in a background of non-channel deposits. The four algorithms can be constrained in different ways, with respect to the choice of distribution types used to parameterize the geometry of the modeled channel bodies (Table 1) and to how the cross-sectional geometry of channel bodies is described (i.e., in terms of width and thickness, width and thickness-to-width aspect ratio, or thickness and width-to-thickness aspect ratio). On this basis, nine different sets of simulations were run by constraining the algorithms with different input types based on the empirical characterization of the studied analogs. Results from these nine sets of simulations are used in the assessment of the modeling algorithms.

Table 1: Distribution types that can be selected for conditioning object-based models, for the chosen algorithms. For each algorithm, the distribution types employed in this work are indicated and highlighted in bold.

	Constant	Uniform	Triangular	Gaussian	Truncated Gaussian	Lognormal	Exponential
FLUVSIM	Yes	Yes	Yes (used)				
TiGenerator	Yes	Yes	Yes (used)				
Tetris	Yes	Yes	Yes (used)	Yes		Yes (used)	Yes
Petrel 2014	Yes	Yes	Yes (used)	Yes	Yes (used)		

2.3 Analysis of model outputs

The output realizations consist of three-dimensional geocellular grids. To quantify the morphometry of the modeled channel bodies, these grids have been analyzed using

software for image analysis (ImageJ; Schneider et al., 2012), through quantification of the modeled architecture in cross sections and in plan-view, as done for the geologic analogs. In this analysis modeling outputs are compared against the same analog dataset on which the input to the models is based. Similarity of the model outputs to the analog data used to define their input is assessed in terms of mean and standard deviation in the morphometric parameters (e.g., thickness, width, planform sinuosity) of the channel bodies. The realizations are additionally compared against the chosen analogs in terms of relationships between pairs of channel-body morphometric parameters, quantified using Pearson's correlation coefficients.

3. Characterization of geologic analogs

The information provided in this section represents a synthesis on frequency distributions, associated descriptive statistics, and relationships, relating to morphometric parameters of analog channel bodies. This information can be applied to constrain object-based models (empirical relationships), and is also used herein to test the modeling algorithms (descriptive statistics and correlations). Both applications are discussed in subsequent sections ('Object-based models: design of the test' and 'Comparison between analogs and models', respectively).

3.1 A note on channel-body geometries and proportions

For analog systems included in the FAKTS database (29 suitable analog subsets), the average size (thickness, width) of channel bodies in stratigraphic intervals commonly increases with increasing proportions of channel deposits (i.e., intervals with larger proportions of channel deposits tend to contain larger channel bodies; Colombera et al., 2016a). This observation might result in part from a genetic relationship between channel-body proportion and geometries (e.g., non-linearity between preservation of channel deposits and preservation of overbank deposits owing to larger and/or more mobile channel belts leading to increased proportion of channel bodies; cf. Bridge and Leeder, 1979). However, because of the way channel bodies are defined in FAKTS, this fact also partially reflects increased likelihood of amalgamation of channel deposits to form larger channelized units.

The results presented in this section are particularly useful for constraining object-based models for fluvial reservoirs that are not characterized by very high proportions of channel deposits. Different approaches would be recommended for modeling high net-to-gross fluvial reservoirs (e.g., modeling non-net objects, such as mud-rich overbank deposits, distributed in channel-deposit background; pixel-based methods).

3.2 Scaling relationships in morphometric parameters

Overall positive relationships between channel-body thickness and width, of variable magnitude, have long been recognized in individual successions (e.g., Robinson and McCabe, 1997; Labourdette and Jones, 2007; Rittersbacher et al., 2014) and in composite datasets compiled from multiple depositional systems (cf. Fielding and Crane, 1987; Reynolds, 1999; Gibling, 2006; Rojas, 2013). It is therefore not surprising that a direct correlation between channel-body width and thickness, albeit weak, is seen across the range of scales of the entire analog data pool (Pearson's $R = 0.31$, $p\text{-value} = 0.00$; Figure 2A). A progressive increase in the width-to-thickness ratio of channel bodies as a function of their scale is also apparent across the entire dataset (Figure 2A); on average, larger (i.e., thicker, wider) channel bodies tend to have larger width-to-thickness ratios than smaller bodies, as previously recognized (cf. Gibling, 2006). However, whereas a positive correlation exists between the width of the channel bodies and their width-to-thickness aspect ratio ($R = 0.79$, $p\text{-value} = 0.00$), no significant correlation is seen between channel-body thickness and width-to-thickness aspect ratio ($R = 0.03$, $p\text{-value} = 0.38$). This is not unexpected, given how these terms appear in the ratios themselves as numerators and denominators. However, it is important to note that this means that channel-body aspect ratios cannot be reliably predicted from thickness alone.

Channel-body width, mean amplitude and mean wavelength also scale to each other. Positive correlation exists between amplitude and wavelength ($R = 0.91$, $p\text{-value} = 0.00$; Figure 2B), amplitude and width ($R = 0.80$, $p\text{-value} = 0.00$; Figure 2C), and wavelength and width ($R = 0.77$, $p\text{-value} = 0.00$; Figure 2D). It is important to stress that the parameters treated here only relate to depositional bodies and not to modern fluvial forms. Scaling involving the wavelength and amplitude of sandbodies is not commonly quantified, due to the limited number of suitable analog studies.

Relationships between river-channel width and measures of wavelength and amplitude that describe the sinuosity of river channels are sometimes considered for purposes of subsurface modeling, as scaling between these quantities is recognized in rivers (Leopold and Wolman, 1960; Williams, 1986). However, these quantities are not necessarily all relevant in application to large-scale channelized sandbodies, as they commonly do not reflect the geometry of the preserved sedimentary products.

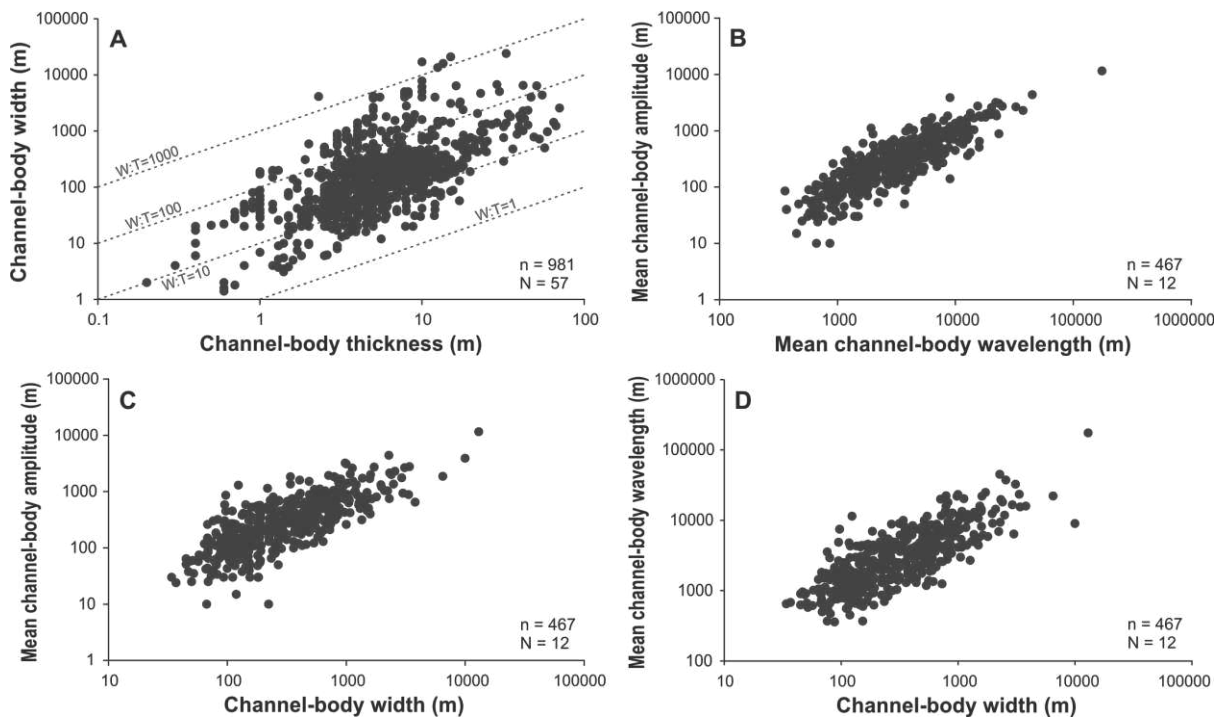


Figure 2: Scatter-plots of morphometric parameters of FAKTS channel bodies from the studied analogs, relating: channel-body width vs thickness (A), mean amplitude vs mean wavelength (B), mean amplitude vs width (C), mean wavelength vs width (D). N = number of subsets; n = number of channel bodies. Axes in logarithmic scale.

3.3 Distributions in morphometric parameters and empirical relationships

Scaling relationships between channel-body thickness, width, mean amplitude and mean wavelength are also expressed in mean values of these parameters across different analog subsets (Figure 3). Empirical relationships have been compiled that can be used in combination to predict averages in channel-body width, mean planform amplitude and mean planform wavelength from average channel-body thickness (Table 2; Figure 3). To further characterize the distribution of these parameters and permit their prediction from partial knowledge of the subsurface,

their minimum and maximum values and their standard deviation have been determined in the studied analogs. Empirical equations have been derived that relate means and standard deviations in channel-body thickness, width, mean amplitude and mean wavelength; these are reported together with associated coefficients of determination in Table 2 and plotted in Figure 4. Additional relationships between means in these parameters and their minimum and maximum values have also been derived, as reported in Table 2; this was done solely because triangular distributions commonly employed to constrain object-based models require definition of minimum and maximum values (see section ‘Object-based models: experimental design of the test’, below).

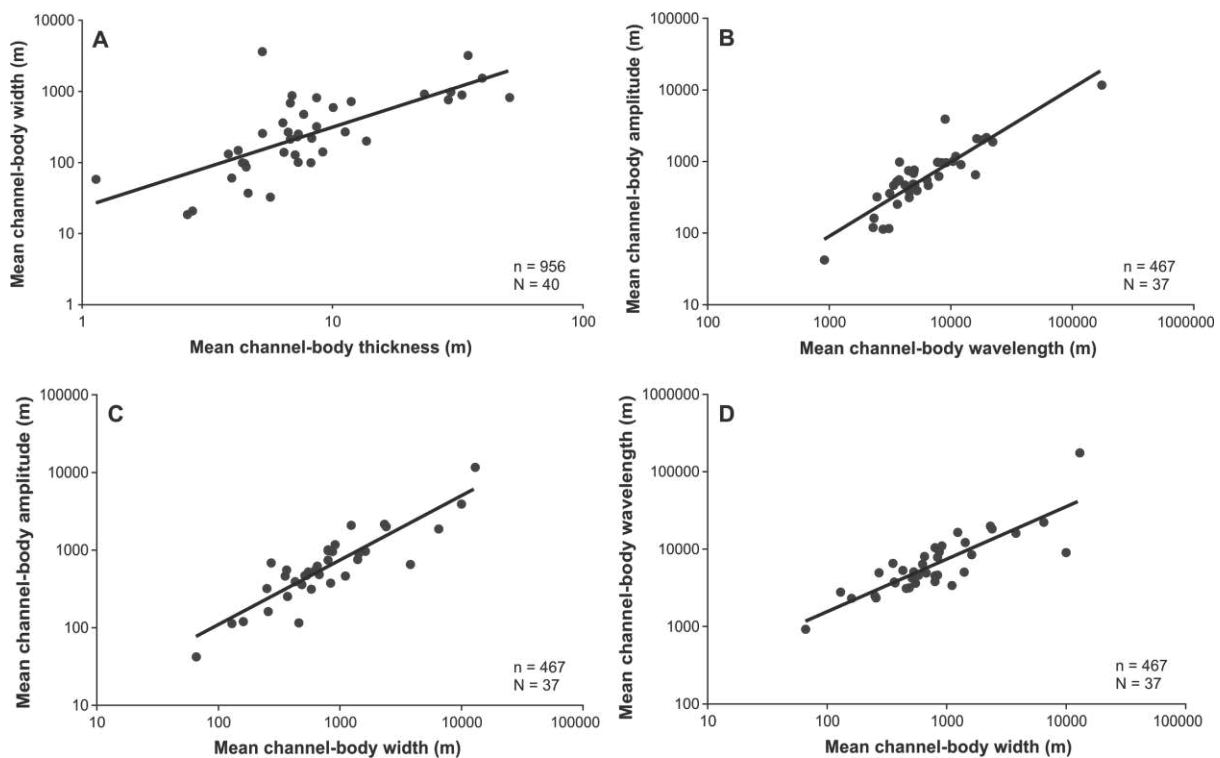


Figure 3: Scatter-plots of averages in morphometric parameters of FAKTS channel bodies from different analog subsets, relating: average channel-body width vs average thickness (A), average mean amplitude vs average mean wavelength (B), average mean amplitude vs average width (C), average mean wavelength vs average width (D). Measures of wavelength and amplitude characterize the plan-view of channel sandbodies as averages of multiple bends of the sinuous planform of each (hence the term ‘mean’); these values are then averaged across the number of sandbodies seen in a studied analog (‘average’). Each data point represents a single FAKTS subset. Best-fit curves correspond to empirical relationships reported in Table 2. The empirical relationships allow selecting input values to object-based modeling algorithms given knowledge of a parameter (e.g., mean thickness of channel bodies). N = number of subsets; n = number of channel bodies. Axes in logarithmic scale.

Table 2: Empirical relationships between descriptive statistics of the morphometric parameters of channel bodies, as based on analysis of the analogs reported in this study. These equations allow derivation of input values to object-based modeling algorithms based on knowledge of a parameter (e.g., mean thickness of channel bodies). Note that FAKTS channel-body amplitude is equal to half the ‘channel amplitude’ of Schlumberger Petrel. CB = channel body; avg = average (relative to the amplitude and wavelength of a single channel body); stdev = standard deviation; T = channel-body thickness; W = channel-body width, A = mean channel-body amplitude; L = mean channel-body wavelength; N = number of subsets; n = number of channel bodies; overscores indicate means; σ = standard deviation. See Figures 3 to 5 for graphical summaries of the data from which these relationships have been derived.

Parameter		Empirical relationship	Coefficient of determination	Data Nr
CB thickness stdev (m)	(1)	$\sigma_T = 0.66 \cdot \bar{T}^{0.93}$	0.73	n = 4,784; N = 174
Mean CB width (m)	(2)	$\bar{W} = 23.41 \cdot \bar{T}^{1.13}$	0.51	n = 956; N = 40
CB width stdev (m)	(3)	$\sigma_W = 0.59 \cdot \bar{W}^{1.05}$	0.90	n = 1,750; N = 34
Mean avg CB amplitude (m)	(4)	$\bar{A} = 2.39 \cdot \bar{W}^{0.83}$	0.77	n = 467; N = 37
	(5)	$\bar{A} = 0.071 \cdot \bar{L}^{1.03}$	0.78	
Avg CB amplitude stdev (m)	(6)	$\sigma_A = 0.80 \cdot \bar{A}^{1.04}$	0.94	n = 449; N = 10
Mean avg CB wavelength (m)	(7)	$\bar{L} = 63.35 \cdot \bar{W}^{0.68}$	0.71	n = 467; N = 37
	(8)	$\bar{L} = 50.83 \cdot \bar{A}^{0.75}$	0.78	
Avg CB wavelength stdev (m)	(9)	$\sigma_L = 0.84 \cdot \bar{L} - 98.58$	0.78	n = 403; N = 10
Min CB thickness (m)	(10)	$\min(T) = 0.35 \cdot \bar{T} - 0.07$	0.69	n = 4,925; N = 109
Max CB thickness (m)	(11)	$\max(T) = 3.04 \cdot \bar{T}^{0.90}$	0.75	
Min CB width (m)	(12)	$\min(W) = 0.55 \cdot \bar{W}^{0.96}$	0.55	n = 1,730; N = 33
Max CB width (m)	(13)	$\max(W) = 6.35 \cdot \bar{W}^{0.89}$	0.88	
Min avg CB amplitude (m)	(14)	$\min(A) = 0$	N/A	n = 449; N = 10
Max avg CB amplitude (m)	(15)	$\max(A) = 5.84 \cdot \bar{A}^{0.95}$	0.80	
Min avg CB wavelength (m)	(16)	$\min(L) = 0.03 \cdot \bar{L}^{1.23}$	0.69	n = 403; N = 10
Max avg CB wavelength (m)	(17)	$\max(L) = 2.98 \cdot \bar{L} + 5214$	0.56	
Mean W/T ratio	(18)	$\bar{r}_{W/T} = 0.11 \cdot \bar{W} + 7.82$	0.94	n = 872; N = 22
W/T ratio stdev	(19)	$\sigma_{r_{W/T}} = 0.29 \cdot \bar{W}^{0.80}$	0.60	
Min W/T ratio	(20)	$\min(r_{W/T}) = 2.09 \cdot \bar{W}^{0.20}$	0.13	
Max W/T ratio	(21)	$\max(r_{W/T}) = 0.48 \cdot \bar{W} + 0.92$	0.91	
Mean T/W ratio	(22)	$\bar{r}_{T/W} = 0.31 \cdot \bar{W}^{-0.31}$	0.33	
T/W ratio stdev	(23)	$\sigma_{r_{T/W}} = 0.10 \cdot \bar{W}^{-0.18}$	0.08	
Min T/W ratio	(24)	$\min(r_{T/W}) = 0.63 \cdot \bar{W}^{-0.76}$	0.59	
Max T/W ratio	(25)	$\max(r_{T/W}) = 0.48 \cdot \bar{W}^{-0.20}$	0.13	

Distributions in channel-body thickness, width, mean planform amplitude and mean planform wavelength almost all exhibit – apart from rare exceptions – positive skewness (overall, 96% of the times; Figure 4). In part, this fact is likely related to a sampling bias, particularly for distributions of channel-body widths. For outcrop analogs, positive skewness might arise because the width of bodies that are wider than the outcrops are not included. However, positively skewed widths are also observed in large outcrop datasets with few or no incomplete measurements. In 3D seismic datasets, positive skewness in morphometric parameters might be due to, or be accentuated by, limits in seismic resolution. Nevertheless, skewed distributions in channel-body geometric parameters appear as a significant characteristic of the studied analogs, which commonly display values of skewness larger than one: it can be argued that skewed distributions are a better choice to describe and model the geometry of channel bodies.

When constraining subsurface models of alluvial architectures, it might be necessary or preferable to work with either width-to-thickness or thickness-to-width aspect ratios. This is necessary when imposed by the specific modeling tool (i.e., it is not possible to constrain distributions in both width and thickness), and preferable when requiring reproduction of scaling factors (i.e., to ensure that bodies that are thicker tend to be wider on average). The width-to-thickness ratio of channel bodies is typically seen to increase with scale (Figure 2A; cf. Fielding and Crane, 1987; Gibling, 2006), and it might therefore be useful to predict descriptive statistics of aspect ratios from channel-deposit thickness statistics. However, poor correlation exists between mean channel-body thickness and both width-to-thickness ($R = -0.07$, $p\text{-value} = 0.74$) and thickness-to-width aspect ratios ($R = -0.23$, $p\text{-value} = 0.29$). Because better correlation exists between channel-body width and width-to-thickness ratios ($R = 0.97$, $p\text{-value} = 0.00$), empirical relationships for predicting how average aspect ratios change with the scale of the channel bodies being modeled are proposed based on knowledge or estimates of mean channel-body width (Table 2; Figure 5A, C). Additional relationships between mean channel-body width and minimum, maximum and standard-deviation values for aspect ratios have also been derived, as reported in Table 2. Distributions in channel-body width-to-thickness and thickness-to-width aspect ratios usually display positive skewness (Figure 5B, D).

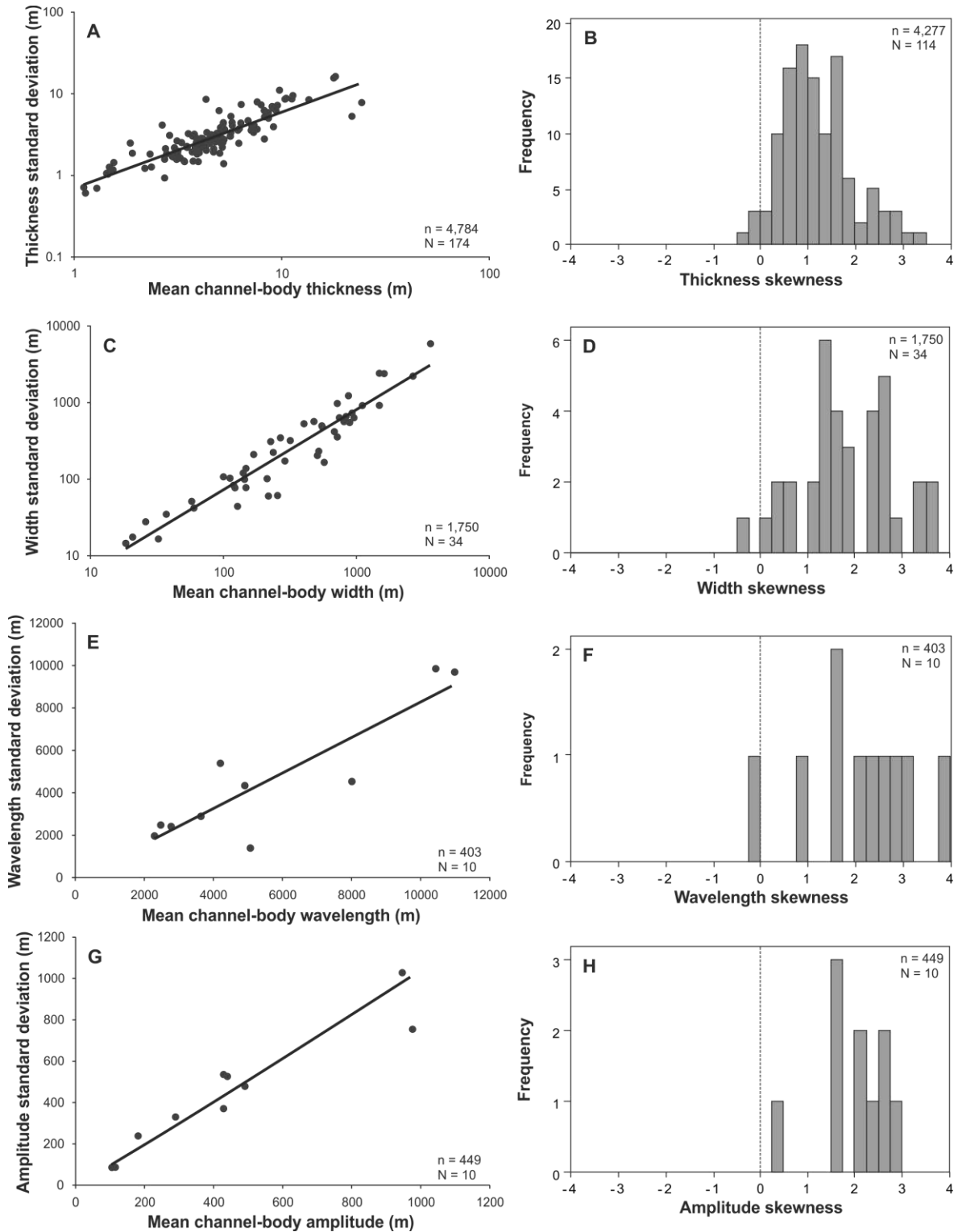


Figure 4: Scatter-plots of mean vs standard deviation (left-hand side), and histograms of skewness in distribution (right-hand side), for morphometric parameters of channel bodies recorded in the FAKTS database from different analog subsets. The morphometric parameters are: channel-body thickness (A, B), width (C, D), mean wavelength (E, F), mean amplitude (G, H). Each data point in the scatter-plots represents a single FAKTS subset. Best-fit curves correspond to empirical relationships reported in Table 2. The empirical relationships allow selecting input values to object-based modeling algorithms given knowledge of a parameter (e.g., mean thickness of channel bodies). N = number of subsets; n = number of channel bodies. Scatter-plot axes in logarithmic scale in parts A and B.

The quantitative tools presented here (Figures 3-5, Table 2) can be applied by geomodelers to constrain object-based models for fluvial reservoirs in absence of other constraints or as alternative scenario.

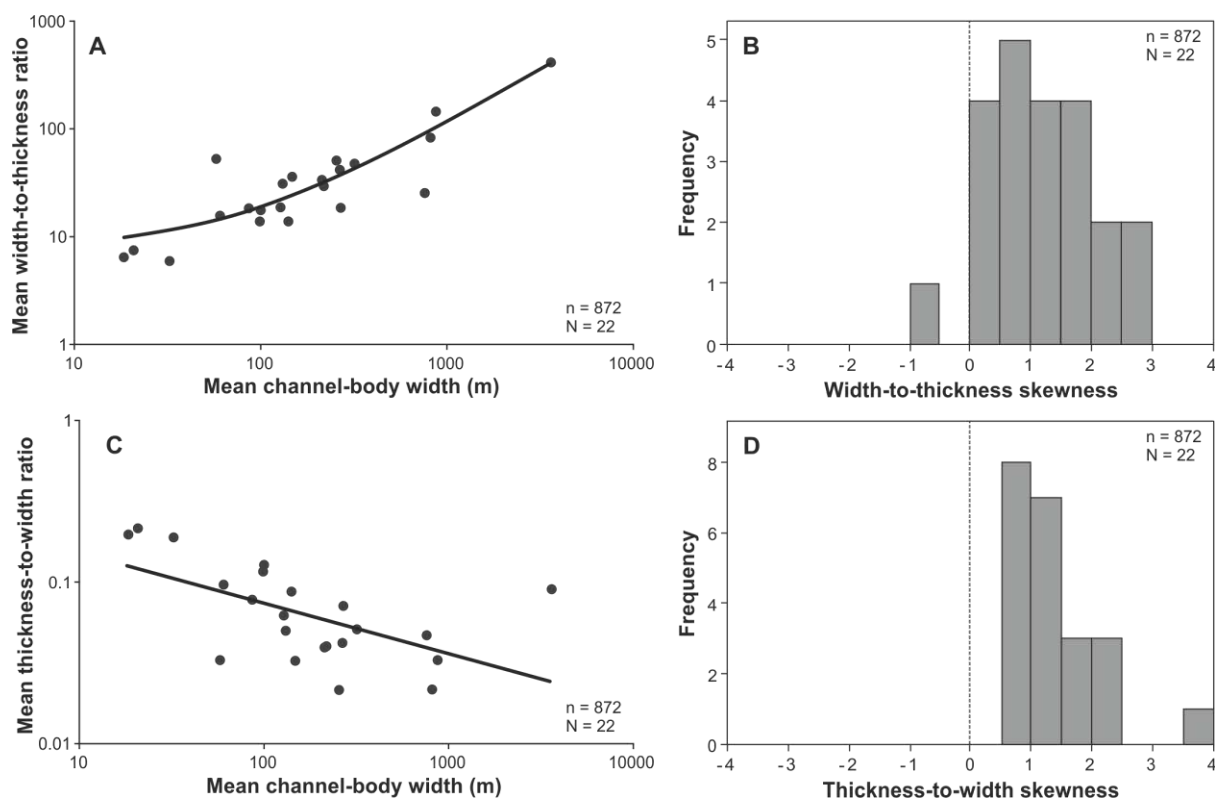


Figure 5: Scatter-plots of mean width vs mean aspect ratio (left-hand side), and histograms of skewness in distribution (right-hand side), for width-to-thickness aspect ratios (A, B) and thickness-to-width aspect ratios (C, D) of channel bodies recorded in the FAKTS database from different analog subsets. Each data point in the scatter-plots represents a single FAKTS subset. Best-fit curves correspond to empirical relationships reported in Table 2. The empirical relationships allow selecting input values to object-based modeling algorithms given knowledge of a parameter (e.g., mean width of channel bodies). N = number of subsets; n = number of channel bodies. Scatter-plot axes in logarithmic scale.

3.4 Variability in correlation between morphometric parameters

Correlation between channel-body thickness, width, mean planform amplitude and mean planform wavelength has been assessed across different analog subsets. Pearson's correlation coefficients indicate moderate or strong positive correlation between these parameters in most stratigraphic successions; their distribution is plotted in Figure 6. By considering several geologic analogs it is possible to quantify

the variability in the magnitude of correlation between the morphometric parameters, expressed by the spread of values in Figure 6. Therefore these quantities provide a benchmark for assessing how well object-based models are able to produce realistic architectures (in section ‘Comparison between analogs and models’).

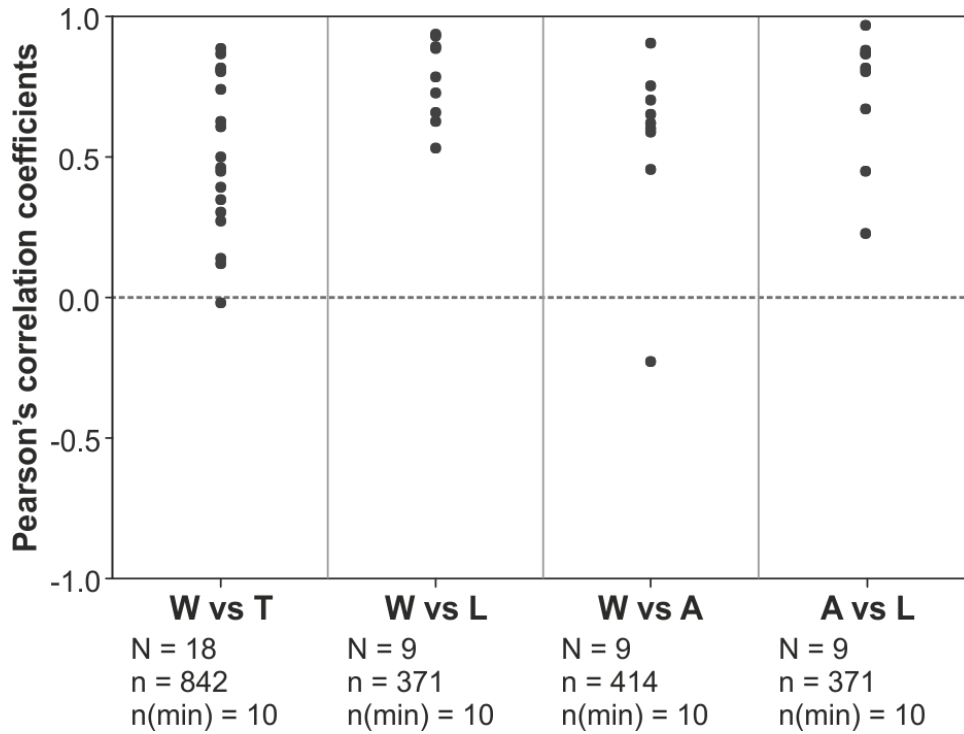


Figure 6: Plots of individual values of Pearson's correlation coefficients for pairs of channel-body morphometric parameters, in FAKTS analog subsets. Each data point in each plot represents a single FAKTS subset. The distributions of correlation coefficients are used in this article to benchmark modeling outputs; they can also be used to inform creation of rules in modeling tools. T = channel-body thickness; W = channel-body width, A = mean channel-body amplitude; L = mean channel-body wavelength; N = number of subsets (corresponding to the number of spots); n = number of channel bodies (total number contained in the N subsets); only subsets with at least 10 channel bodies are considered.

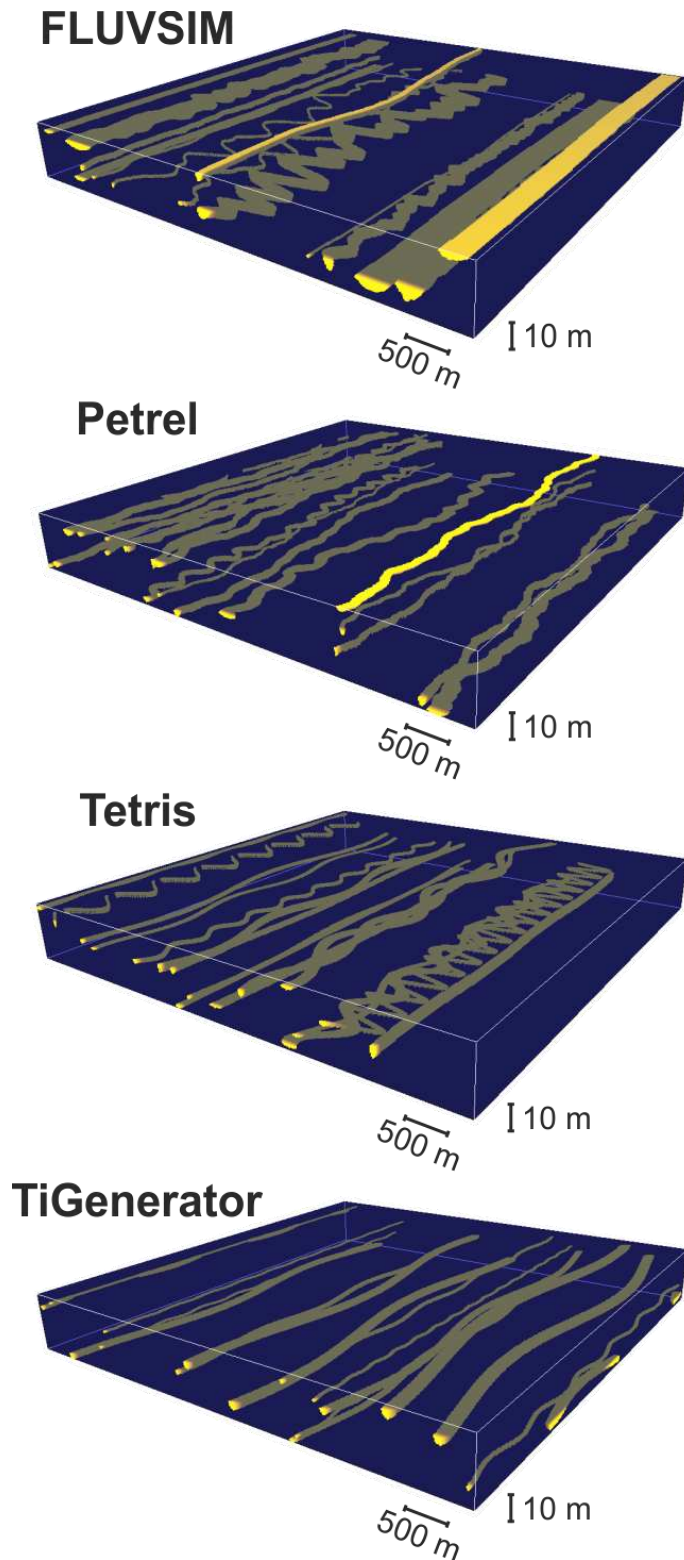


Figure 7: Perspective view of example realizations generated using the different object-based algorithms (as labelled), through input parameters associated with the same modeling scenario (scenario1; Tables 3 and 4). Although the input relates to the same scenario, specific input parameters might differ (e.g., by constraining channel-body widths and thicknesses in the form of distributions in width and thickness, thickness and width-to-thickness aspect ratio, or width and thickness-to-width aspect ratio; see text). Channel bodies appear in yellow; the rest of the volume is transparent. This figure highlights how input based on corresponding analog data can translate in strikingly different output.

4. Object-based models: design of the test

To test the four modeling algorithms, nine modeling strategies were employed that consider their application by constraining the models using different distribution types (Table 1) and alternative ways to describe channel-body cross-sectional geometries (i.e., by distributions in channel-body width and thickness, or aspect ratios; Tables 3-5). Thickness-to-width and width-to-thickness aspect ratios can be used as input to Petrel and FLUVSIM, respectively. So, the nine modeling approaches chosen to test the algorithms can be summarized as follows:

- FLUVSIM (triangular distributions; thickness and width-to-thickness aspect ratio; overall aspect-ratio statistics based on Table 4)
- FLUVSIM (triangular distributions; thickness and width-to-thickness aspect ratio; aspect-ratio statistics predicted empirically based on Table 5 – only 2D)
- Petrel (triangular distributions; width and thickness-to-width aspect ratio; overall aspect-ratio statistics based on Table 4)
- Petrel (triangular distributions; width and thickness-to-width aspect ratio; aspect-ratio statistics predicted empirically based on Table 5 – only 2D)
- Petrel (triangular distributions; thickness and width)
- Petrel (truncated Gaussian distributions; thickness and width – only 2D)
- Tetris (triangular distributions; thickness and width)
- Tetris (lognormal distributions; thickness and width)
- TiGenerator (triangular distributions; thickness and width)

Triangular, lognormal and truncated Gaussian distributions were adopted because they can replicate the positive skewness in channel-body morphometry seen in the analogs (Figure 4).

Table 3: Sets of channel-body parameter values for the six modeling scenarios, which reflect increasing scale in the size of the modeled channel bodies. Percentiles of channel-body mean thickness are based on subsets with at least 15 channel bodies. These values of thickness are taken as mean thickness for channel body populations, to which empirical relationships (Table 2) are applied to predict distributions of other parameters, in order to define the different scenarios. Modes in channel-body parameters for the six scenarios, used to define triangular distributions, are calculated based on mean and standard deviation, and assuming a lognormal distribution ($\text{mode}(x) = e^{(\text{location} - \text{scale}^2)}$) for the parameters in the studied analogs. Mean-thickness statistics based on: $n = 5,018$ channel bodies; $N = 112$ subsets. Each percentile of all data is taken as a mean thickness for each scenario. CB = channel body; stdev = standard deviation; min = minimum; max = maximum.

Scenario		1	2	3	4	5	6
Thickness statistics	Statistic	5 th centile	25 th centile	Median	Mean	75 th centile	95 th centile
	Value (m)	1.6 m [5.2 ft]	3.6 m [11.8 ft]	5.3 m [17.4 ft]	6 m [19.7 ft]	7.1 m [23.3 ft]	13.2 m [43.3 ft]
Predicted CB thickness stdev (m)		1 m [3.3 ft]	2.2 m [7.2 ft]	3.1 m [10.2 ft]	3.5 m [11.5 ft]	4.1 m [13.5 ft]	7.3 m [24 ft]
Predicted mean CB width (m)		40 m [131.2 ft]	100 m [328.1 ft]	154 m [505.2 ft]	177 m [580.7 ft]	214 m [702.1 ft]	432 m [1417.3 ft]
Predicted CB width stdev (m)		28 m [91.9 ft]	74 m [242.8 ft]	117 m [383.9 ft]	136 m [446.2 ft]	165 m [541.3 ft]	345 m [1131.9 ft]
Predicted mean CB amplitude (m)		51 m [167.3 ft]	109 m [357.6 ft]	156 m [511.8 ft]	176 m [577.4 ft]	206 m [675.9 ft]	368 m [1207.3 ft]
Predicted CB amplitude stdev (m)		48 m [157.5 ft]	105 m [344.5 ft]	153 m [502 ft]	173 m [567.6 ft]	204 m [669.3 ft]	373 m [1223.8 ft]
Predicted mean CB wavelength (m)		776 m [2545.9 ft]	1447 m [4747.4 ft]	1947 m [6387.8 ft]	2142 m [7027.6 ft]	2438 m [7998.7 ft]	3926 m [12880.6 ft]
Predicted CB wavelength stdev (m)		715 m [2345.8 ft]	1340 m [4396.3 ft]	1790 m [5872.7 ft]	1962 m [6437 ft]	2221 m [7286.7 ft]	3490 m [11450.1 ft]
Predicted CB thickness min (m)		0.5 m [1.6 ft]	1.2 m [3.9 ft]	1.8 m [5.9 ft]	2 m [6.6 ft]	2.4 m [7.9 ft]	4.6 m [15.1 ft]
Predicted CB thickness max (m)		4.6 m [15.1 ft]	9.6 m [31.5 ft]	13.6 m [44.6 ft]	15.2 m [49.9 ft]	17.7 m [58.1 ft]	31 m [101.7 ft]
Predicted CB width min (m)		19 m [62.3 ft]	46 m [150.9 ft]	69 m [226.4 ft]	79 m [259.2 ft]	95 m [311.7 ft]	186 m [610.2 ft]
Predicted CB width max (m)		169 m [554.5 ft]	381 m [1250 ft]	562 m [1843.8 ft]	637 m [2089.9 ft]	754 m [2473.8 ft]	1408 m [4619.4 ft]
CB amplitude min (m)		0 m [0 ft]	0 m [0 ft]	0 m [0 ft]	0 m [0 ft]	0 m [0 ft]	0 m [0 ft]
Predicted CB amplitude max (m)		244 m [800.5 ft]	503 m [1650.3 ft]	710 m [2329.4 ft]	793 m [2601.7 ft]	921 m [3021.7 ft]	1600 m [5249.3 ft]
Predicted CB wavelength min (m)		108 m [354.3 ft]	231 m [757.9 ft]	334 m [1095.8 ft]	375 m [1230.3 ft]	440 m [1443.6 ft]	790 m [2591.9 ft]
Predicted CB wavelength max (m)		7526 m [24691.6 ft]	9525 m [31250 ft]	11017 m [36145 ft]	11598 m [38051.2 ft]	12479 m [40941.6 ft]	16915 m [55495.4 ft]
Predicted CB thickness mode (m)		1 m [3.3 ft]	2.3 m [7.5 ft]	3.4 m [11.2 ft]	3.9 m [12.8 ft]	4.6 m [15.1 ft]	8.9 m [29.2 ft]
Predicted CB width mode (m)		22 m [72.2 ft]	52 m [170.6 ft]	78 m [255.9 ft]	89 m [292 ft]	106 m [347.8 ft]	206 m [675.9 ft]
Predicted CB amplitude mode (m)		20 m [65.6 ft]	41 m [134.5 ft]	57 m [187 ft]	64 m [210 ft]	74 m [242.8 ft]	128 m [419.9 ft]
Predicted CB wavelength mode (m)		309 m [1013.8 ft]	571 m [1873.4 ft]	777 m [2549.2 ft]	859 m [2818.2 ft]	985 m [3231.6 ft]	1640 m [5380.6 ft]

Table 4: Values of minimum, maximum, mean, and standard deviation in thickness-to-width (T/W) and width-to-thickness (W/T) aspect ratios, used as input to Petrel and FLUVSIM models respectively, based on averages across the entire analog datasets. These aspect ratios have been applied constantly across the range of scales modeled in the six scenarios. Statistics based on: n = 924 channel bodies; N = 30 subsets. Sc. Nr. = scenario number. Modes in aspect ratios have been computed for values of mean and standard deviation assuming the distributions to be lognormal.

Scenario	Min T/W ratio	Max T/W ratio	Mean T/W ratio	T/W ratio stdev	Mode T/W ratio	Min W/T ratio	Max W/T ratio	Mean W/T ratio	W/T ratio stdev	Mode W/T ratio
1 to 6	0.02	0.07	0.18	0.05	0.04	10.5	52.9	169.8	45.2	23

Table 5: Values of minimum, maximum, mean, and standard deviation in thickness-to-width (T/W) and width-to-thickness (W/T) aspect ratios, used as input to simulations run with Petrel and FLUVSIM respectively, based on predictions using empirical relationships (equations 18-25 in Table 2) and mean channel-body widths for the six scenarios (Table 3). Modes in aspect ratios have been computed for values of mean and standard deviation assuming the distributions to be lognormal.

Scenario	Min T/W ratio	Max T/W ratio	Mean T/W ratio	T/W ratio stdev	Mode T/W ratio	Min W/T ratio	Max W/T ratio	Mean W/T ratio	W/T ratio stdev	Mode W/T ratio
1	0.04	0.23	0.10	0.05	0.07	4.37	20.12	12.2	5.6	9.2
2	0.02	0.19	0.07	0.04	0.05	5.25	48.92	18.8	11.6	11.7
3	0.01	0.18	0.07	0.04	0.04	5.72	74.84	24.8	16.3	14.4
4	0.01	0.17	0.06	0.04	0.04	5.88	85.88	27.3	18.2	15.7
5	0.01	0.16	0.06	0.04	0.03	6.11	103.64	31.4	21.2	17.8
6	0.01	0.14	0.05	0.03	0.03	7.03	208.28	55.3	37.2	31.6

The employed modeling approaches were chosen because they reflect different combinations of choices that modelers need to make when constraining object-based models. Each of the nine modeling approaches were applied to six different sets of parameters ('scenarios' hereafter). Each parameter set is built using the empirical relations presented above (Table 2, Figures 3 and 4), applied to different values of mean channel-body thickness, themselves chosen to reflect the average, the median and significant percentiles (5, 25, 75, 95) of the entire data pool of channel bodies (FAKTS subsets containing at least 15 channel bodies). These six scenarios of increasing channel-body size were chosen to cover the broad range of scales of channelized alluvial architectures seen in the rock record. The type of input parameters (e.g., min., mode and max. vs mean and standard deviation) varies

depending on requirements of each algorithm and chosen modeling strategy. Since distributions in channel-body geometries tend to be positively skewed, modes were computed from values of mean and standard deviation assuming all distributions to be lognormal (the mode of a lognormal distribution is equal to $e^{\text{location}-\text{scale}^2}$, where location and scale parameters are the mean and standard deviation of the natural logarithm of the variable at hand; location and scale can be derived from values of mean and standard deviation of the variable itself). All parameters for distributions in channel-body geometries (thickness, width, mean amplitude and mean wavelength) used to constrain the models for the six scenarios are reported in Table 3. Input parameters for width-to-thickness and thickness-to-width ratios were first chosen based on descriptive statistics from the whole channel-body data pool, as reported in Table 4. In this case, aspect ratios were applied constantly over the entire range of scales (i.e., the six scenarios), as no significant relationship was seen between mean channel-body thickness and mean width-to-thickness ratio, nor between mean thickness and mean thickness-to-width ratio, in the studied analogs. However, this will affect comparisons with simulations modeled using width distributions, given that the applied relationships return a 31% increase in the ratio between predicted mean width and mean thickness across the six scenarios (Table 3). Thus, two additional sets of simulations were constrained assuming aspect-ratio descriptive statistics to vary over the range of scales of the six scenarios, as seen in the analogs (Figure 2A), again by applying empirical relations (Table 2, Figure 5), as reported in Table 5.

Ten simulations were run for each scenario and modeling strategy, returning gridded realizations that appear in the form of the representative examples depicted in Figure 7. On average, each realization contains 9.9 fully measurable channelized units. The simulation grids scale to the size of the units modeled therein, ranging in volume from $7.5 \cdot 10^7 \text{ m}^3$ (scenario 1) to $7.8 \cdot 10^9 \text{ m}^3$ (scenario 6). To increase the sample of channel bodies measurable in cross section, each simulation was run on larger 2D strike-oriented sections, which increase in area from $2 \cdot 10^4 \text{ m}^2$ to $1.1 \cdot 10^6 \text{ m}^2$. The adoption of large grids minimizes problems of volume support in the statistics of the measured channel-body morphometry.

5. Comparison between analogs and models

Outputs from the nine sets of object-based models are here compared against the characteristics recognized in the analogs from FAKTS. Comparisons are made for (i) descriptive statistics of distributions in channel-body geometries and (ii) correlation coefficients relating to pairs of the same geometric parameters.

5.1 Distributions in morphometric parameters

Values of mean and standard deviation of morphometric parameters of the modeled channel bodies across each set of ten realizations (i.e., for the six scenarios) are compared with corresponding values derived from the analog-based empirical relationships (Table 2) used to define the model input (Table 3). Although it might seem intuitive that the output should match the corresponding values derived from the empirical relationships and on which the input to the models themselves is based, some discrepancy might exist for the following reasons: (i) the form in which the input is defined (e.g., as minimum, mode and maximum versus mean and standard deviation); (ii) the output error within a range that is considered an acceptable match by the algorithms; (iii) limited sample (i.e., realization) size; and (iv) measurement error in image analysis.

With increasing scale (i.e., from scenario 1 to 6), the discrepancy between values of mean and standard deviation in the thickness of the modeled channel bodies and corresponding analog-based target values increases if the discrepancy is considered in terms of differences in absolute values, but displays modest change if expressed as ratio between the values (Figure 8A, B). The discrepancy between target values and model outputs is significantly larger for models conditioned on thickness-to-width aspect ratios using Petrel, in comparison to models constrained on channel-body thickness distributions reaching a discrepancy by factors up to 4.3 and 5.2 for mean and standard deviation (Figure 8A, B). Overall, a closer match between model outputs and analog values is seen for models constrained using thickness-to-width aspect-ratio statistics that are assumed to vary with scale (Figure 9A, B).

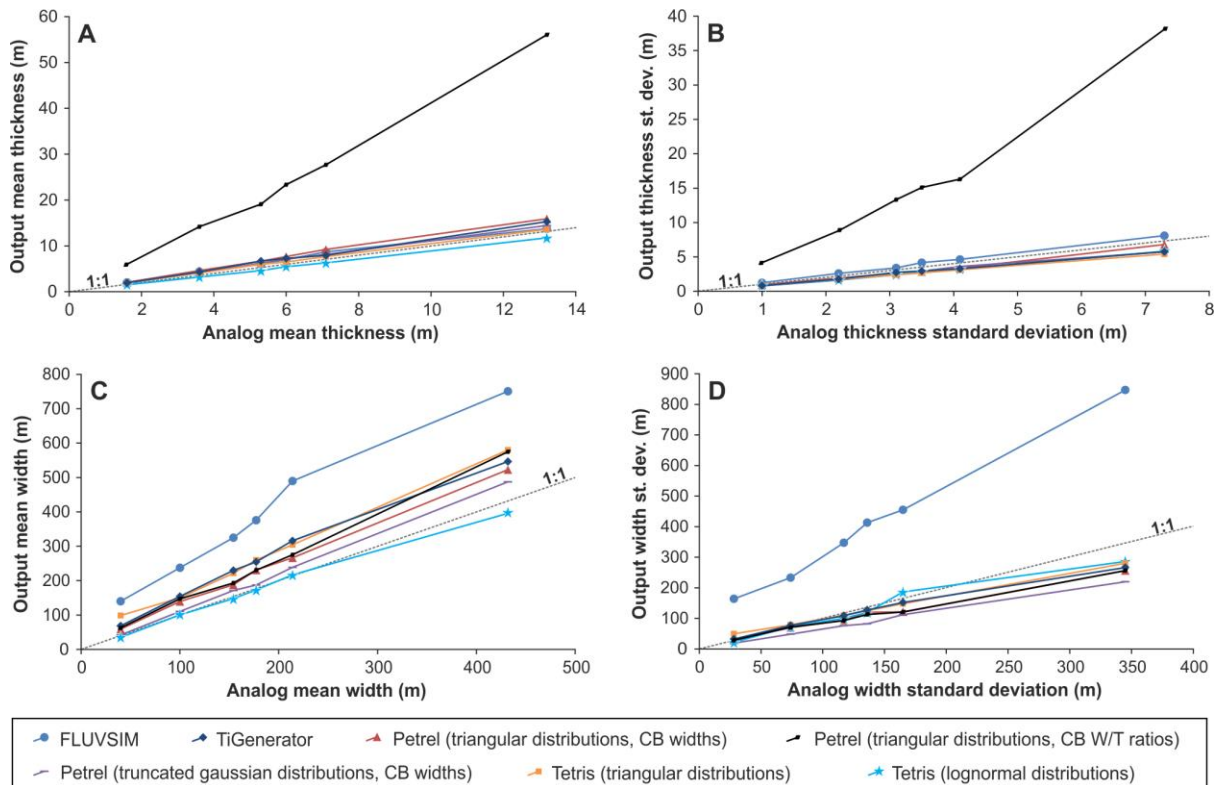


Figure 8: Cross-plots of descriptive statistics (mean, standard deviation) of channel-body thickness (A, B) and width (C, D) in different sets of object-based models vs those predicted by the empirical relationships and used to define the model inputs, for the six modeling scenarios (i.e., for increasing scale, from left to right in each plot). For models constrained using channel-body aspect-ratio statistics, the results shown here only relate to realizations for which input aspect-ratio statistics were kept constant in all scenarios (Table 4). Data on realizations constrained using channel-body aspect-ratio statistics that are assumed to vary with scale are separately reported in Figure 9. Each value of mean or standard deviation relating to the model outputs incorporate statistics from all ten simulations run for each scenario. CB = channel body; W/T = width-to-thickness aspect ratio. In each case, a perfect match between analog-based targets and model output would follow the 1:1 line.

Across the six scenarios of channel-body scale, the modeling outputs include bodies that are on average wider than what is predicted by the empirical relationships used to define the input; this is true for models built with any of the modeling strategies except those constructed using Tetris and conditioned on lognormally distributed widths (Figure 8C). This observation contrasts with what is expected if issues of sample size arose, in relation to the increased likelihood for the margins of the largest channel bodies to occur outside the modeled volume. The discrepancy between the mean and standard deviation in the width of modeled channel bodies and the corresponding values from the analog-based relationships increases with increasing channel-body scale (i.e., from scenario 1 to 6; Figure 8C, D) if considered in terms of differences of absolute values. However, this discrepancy tends to

decrease if treated as a ratio between the same values. The discrepancy between analog-based values and model outputs is significantly larger for models conditioned on width-to-thickness aspect ratios, i.e., using FLUVSIM, in comparison to models constrained on channel-body width distributions, by factors up to 3.9 and 5.9 for mean and standard deviation values, respectively, for the scenario 1 (Figure 8C, D). For scenarios 1 to 4, a closer match between model outputs and analog-based target values is seen for models constrained using width-to-thickness aspect-ratio statistics that are assumed to vary with scale (Figure 9A, B). Models run using Tetris by employing lognormal distributions of channel-body morphometric parameters, and so conditioned on values of mean and variance, return the best match between model output and analog-based targets for measures of channel-body width (Figure 8C, D).

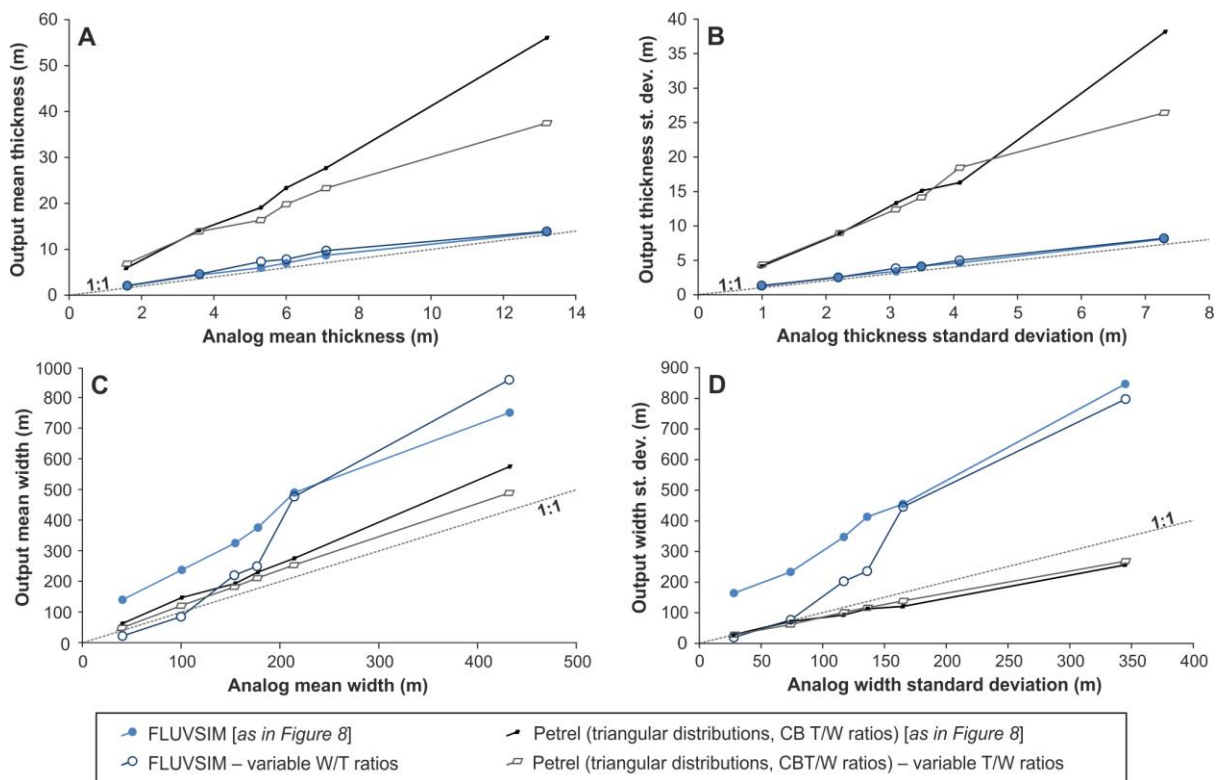


Figure 9: Cross-plots of mean and standard deviation of channel-body thickness (A, B) and width (C, D) in sets of object-based models conditioned on aspect ratios vs values predicted by the empirical relationships and used to define the model inputs, for the six modeling scenarios (i.e., for increasing scale, from left to right in each plot). Simulations constrained assuming changes in descriptive statistics of the aspect ratios with scale (Table 5) are compared against simulations for which inputs describing aspect ratios were kept constant in all scenarios (Table 4). Each value of mean or standard deviation relating to the model outputs incorporate statistics from all ten simulations run for each scenario. CB = channel body; W/T = width-to-thickness aspect ratio. In each case, a perfect match between analog-based targets and model output would follow the 1:1 line.

FLUVSIM and Petrel reproduce channelized units with wavelength and amplitude that vary along the length of each body, which makes their output comparable to geometries observed in the studied fluvial systems. By contrast, Tetris and TiGenerator only create simple sinusoids, each having effectively constant wavelength and amplitude.

Except for models generated with Tetris and using lognormal distributions, the mean wavelength of modeled channel bodies is consistently larger than what is predicted by the relationships used to define the input, on average 1.9 times (Figure 10A). Models run using distributions defined on mean and standard deviation (i.e., created with Petrel using truncated normal distributions, and Tetris using lognormal distributions) produce channel bodies with less variable wavelength than what is expected based on the empirical relationships, whereas other algorithms tend to return more variable wavelength (Figure 10B).

The ‘mean amplitude’ of modeled channel bodies is, in most cases (26 out of 36 sets of realizations), on average larger than target values based on the empirical relationships (on average 1.24 times, but up to 1.64 times; Figure 10C), but is usually less variable (Figure 10D).

When all the parameters are considered simultaneously, the best overall match between the modeled and analog-based values of mean and standard deviation in channel-body morphometric parameters is returned by models created by Tetris (when conditioned on lognormal distributions; average overall discrepancy across all realizations and the six scenarios: 20%), followed by Petrel (when conditioned on truncated normal distributions; overall discrepancy: 36%), TiGenerator (overall discrepancy: 38%), and FLUVSIM (overall discrepancy of 45% if aspect-ratio statistics vary across the six scenarios, i.e., with scale; 69% otherwise). All the algorithms reproduce distributions of channel-body widths or amplitudes (or both) with mean values larger than those predicted on the basis of the relationships used to define the input. This is significant given the importance of these parameters in controlling the horizontal connectivity of channel deposits.

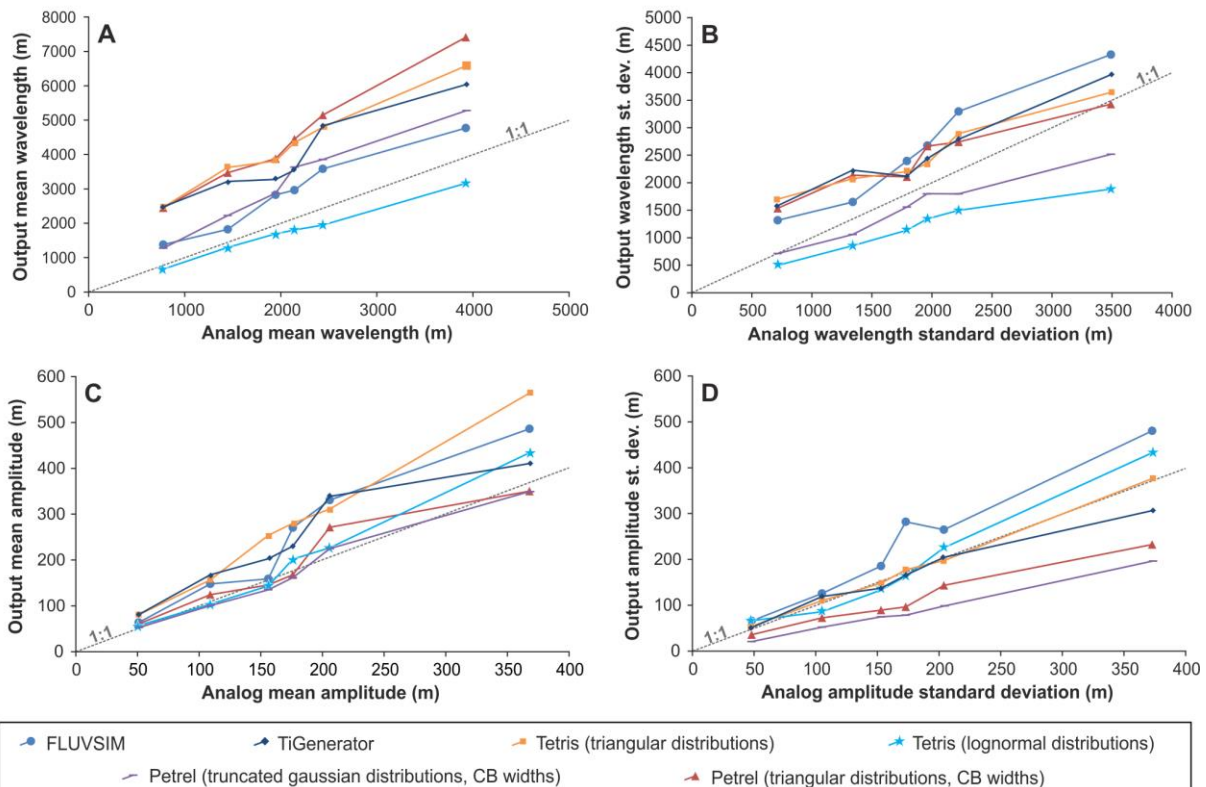


Figure 10: Cross-plots of descriptive statistics (mean, standard deviation) of channel-body mean wavelength (A, B) and amplitude (C, D) in the different sets of object-based models vs those predicted by the empirical relationships and used to define the model inputs, for the six modeling scenarios (i.e., for increasing scale, from left to right in each plot). Each value of mean or standard deviation relating to the model outputs incorporate statistics from all ten simulations run for each scenario. CB = channel body. In each case, a perfect match between analog-based targets and model output would follow the 1:1 line.

5.2 Correlations between morphometric parameters

Relationships between the channel-body morphometric parameters are assessed for each realization, and quantified by Pearson's correlation coefficients. The distributions of Pearson's R values across the 60 realizations run with each modeling strategy and across the six modeling scenarios are compared with those computed for the FAKTS analogs (Figure 11).

Near-to-perfect positive linear relationships (i.e., Pearson's Rs close to 1.0) between all the parameters (width vs thickness, width vs mean wavelength, width vs mean amplitude, mean amplitude vs mean wavelength) are seen in outputs from TiGenerator; these R values far exceed those observed in the studied analogs (Figure 11). On the contrary, based on mean and median R values, on average no relationship is seen between any of the parameters in outputs from Tetrism (Figure

11), in which the relationships between the modeled parameters are negative in 46% of the cases.

Realizations generated using FLUVSIM and Petrel, and constrained on aspect ratios demonstrate consistently positive relationships between channel-body width and thickness, in agreement with observations from the analogs (Figure 11A). For correlations between channel-body widths and thicknesses, the distribution of R values in FLUVSIM models has a mean (0.56) that is not statistically different from the mean (0.51) in the distribution in R seen in the analogs from FAKTS (2-sample t-test: $T = -0.69$, $p\text{-value} = 0.497$, $d.f. = 24$); instead the mean R value in Petrel models constructed using thickness-to-width ratios (0.70) is larger than the mean R seen in the analogs to a statistically significant level (2-sample t-test: $T = -2.68$, $p\text{-value} = 0.015$, $d.f. = 19$).

When relationships between channel-body width and mean wavelength, and between width and mean amplitude are investigated, with the exception of TiGenerator, all the algorithms return realizations with both positive and negative, usually weak, relationships, and with distributions in R values whose mean is close to zero.

When relationships between mean wavelength and mean amplitude are considered, models built using Petrel tend to display positive relationships, as observed in the analogs, with distributions in R values that are on average significantly different from zero (1-sample t-test for models conditioned on triangular distributions: $T = 5.40$, $p\text{-value} = 0.000$, $d.f. = 59$; 1-sample t-test for models conditioned on truncated normal distributions: $T = 12.15$, $p\text{-value} = 0.000$, $d.f. = 59$) but also significantly different from the corresponding distribution for the analogs (2-sample t-test for models conditioned on triangular distributions: $T = 5.56$, $p\text{-value} = 0.000$, $d.f. = 12$; 2-sample t-test for models conditioned on truncated normal distributions: $T = 3.80$, $p\text{-value} = 0.003$, $d.f. = 10$).

Apart from those created with TiGenerator, all models show some variability in R values over the six scenarios (i.e., scales), when the ten realizations for each are considered jointly (Figure 11B, D, F, H).

None of the modeling algorithms fully reproduces the correlations between channel-body morphometric parameters seen in nature.

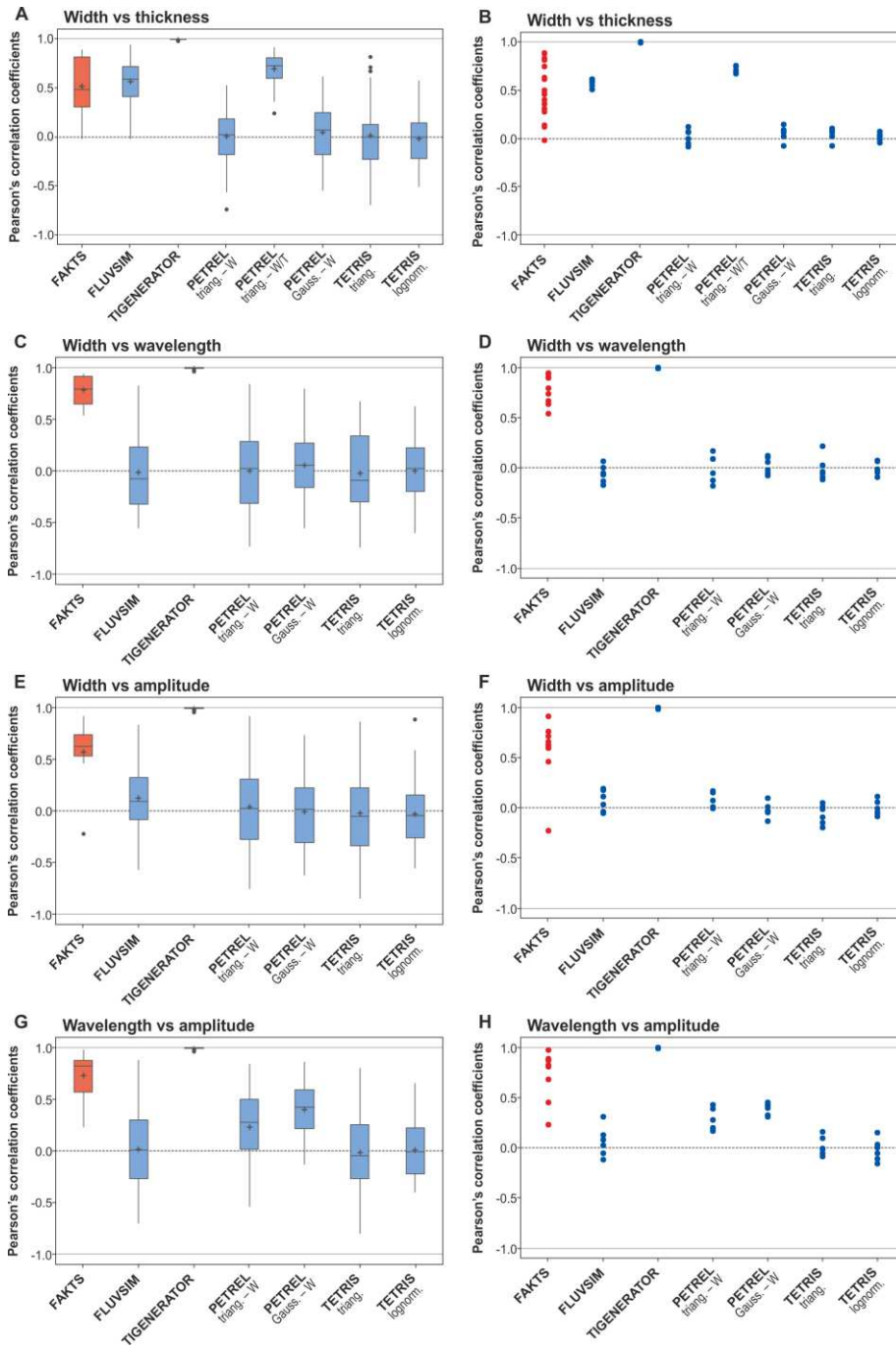


Figure 11: Left-hand side: box-plots that relate the distribution of Pearson's correlation coefficients for pairs of channel-body morphometric parameters, in all realizations for each modeling approach. Boxes represent interquartile ranges, horizontal bars within them represent median values, '+' signs represent mean values, and spots represent outliers. Right-hand side: plots of individual values of Pearson's correlation coefficients for pairs of channel-body morphometric parameters, in all realizations for each modeling approach and scenario. Relationships are assessed between channel-body width and thickness (A, B), width and mean wavelength (C, D), width and mean amplitude (E, F), and mean wavelength and mean amplitude (G, H). Model outputs (blue) are compared with analogs in FAKTS (red). The plots on the right-hand side illustrate variability in correlation across all 60 realizations created with each modeling strategy, compared against the analog observations; the plots on the right-hand side illustrate variability across the six modeling scenarios for each modeling strategy, compared against the analog observations. Triang. = models constrained on triangular distributions; Gauss. = models constrained on truncated Gaussian distributions; lognorm. = models constrained on lognormal distributions; W = models constrained on channel-body widths; W/T = models constrained on channel-body width-to-thickness aspect ratios.

6. Discussion

For object-based models of fluvial reservoirs or aquifers, geologic realism relies on suitable constraints of the cross sectional and planform geometries of large-scale channel bodies. Geologic analogs are commonly considered for this purpose, and this approach is sensible whenever analogs can be chosen with some confidence (e.g., Bridge et al., 2000; Norden and Frykman, 2013). However, selection of appropriate analogs is not trivial (Alexander, 1993; Howell et al., 2014; Ringrose and Bentley, 2015), and the capacity to source appropriate data is limited by available time and resources. Also, analog datasets based on single examples may not be representative of a most-likely scenario, given the variability in sedimentary architecture seen among depositional systems of the same type (cf. Colombera et al., 2013). Additionally, for fluvial channelized sandbodies in particular, the scarcity of suitable data on the planform geometry of the bodies has, in some cases, led modelers to misuse data on the geomorphology of modern river systems (e.g., sinuosity of active river channels), with no consideration of the extent to which modern forms differ from the geometry of bodies preserved in the stratigraphic record (Kerrou et al., 2008; Larriestra and Gomez, 2010; Zovi et al., 2017). In view of these problems, more comprehensive compilations of information from geologic analogs that can be used in subsurface modeling have long been advocated (Dagan, 2002; de Marsily et al., 2005; Rubin et al., 2006; Ronayne et al., 2008).

As a way to partly address these problems, the empirical characterization undertaken here provides relationships that can be used in subsurface modeling contexts when geologic-analog data are lacking, or when alternative analogs are sought to assess uncertainty in predictions. The equations in Table 2 represent a synthesis of information on the morphometric scaling of fluvial channel bodies as seen in 61 analog studies. They therefore form a set of constraints that can be applied in data-poor situations of subsurface characterization, possibly as a base-case scenario. In principle, the empirical relationships can be used based on knowledge of channel-deposit thicknesses as observed in borehole data. Nonetheless, it must be borne in mind that the ability to compare subsurface and analog datasets is affected by lateral variability in the thickness of channel bodies and by channel-body amalgamation. Also, the underlying dataset (cf. Figure 2)

highlights the fact that establishing alternative scenarios based on ranges in morphometric parameters is advisable for handling uncertainty.

The data and empirical relations presented here are based on a synthesis of sedimentologic studies on fluvial successions of any nature, without any effort to focus the scope of investigation on depositional systems developed under particular conditions (e.g., depositional environment, climate type, discharge regime, geologic age). A synthesis of this type is helpful in situations where subsurface data are scarce or of limited value for sedimentologic interpretations, and where therefore any interpretation of the type of fluvial system that deposited a succession is difficult to attempt; in such case, it is convenient to consider a base-case scenario. For situations in which, instead, geologic data allow interpretation of the depositional context of a fluvial succession, similar relationships for classified depositional systems are desirable, as these would have higher predictive power (cf. Colombera et al., 2014). However, a comprehensive compilation would require substantial additional data collection, which is beyond the scope of this study.

All the above reflects the expectation that using suitable analog data will result in subsurface models that are more realistic, ignoring that this might not always be true because of limitations in the modeling tools. The comparative analysis conducted here provides insight into the degree to which different object-based modeling methods are able to reproduce characteristics that are expected in the channelized architecture of fluvial aquifers or reservoirs. An assessment was made of the following: (i) how faithfully descriptive statistics of channel-body morphometry in the model outputs match with the descriptive statistics that either constitute the input to the models or form the basis on which the input is defined; (ii) whether realistic scaling relationships between the different morphometric parameters are reproduced in the simulations. All the tested methods have shown problems in several of the aspects considered. For example, to achieve positive scaling between channel-body thickness and width, constraining models using aspect ratios is recommended when working with FLUVSIM and Petrel (Figure 11). However, doing so by employing analog-informed distributions of aspect ratios resulted in less realistic distributions of thickness and width (Figures 8 and 9), respectively, compared to models for which the input was defined by channel-body thickness and width distributions.

The existence of such a technical bias means that the application of realistic input parameters to stochastic modeling methods does not necessarily result in entirely realistic outputs. Therefore, it is not possible to provide universal guidelines on the use of object-based modeling algorithms and training-image generators. It is merely possible to warn against the types of misrepresentations that might arise by adopting a particular tool in a certain way, particularly if the proposed empirical relationships were applied. These issues are all expressed in quantitative form in the results of this work, and in particular in Figures 8 to 11, for the broad spectrum of scales at which fluvial channel deposits accumulate. These results can be used by geomodelers to predict and communicate the specific characteristics of object-based models of the subsurface that are not likely to be geologically realistic. Knowing the limitations of a particular method is useful because, depending on the type of subsurface problem under consideration, it might be preferable to use algorithms that appear to reproduce more accurate distributions and relationships for parameters that are known to exert a stronger control on sandbody connectivity along a direction of interest (i.e., width and amplitude in horizontal directions, and thickness in the vertical direction; cf. Hovadik and Larue, 2007; de Jager et al., 2009; Jha et al., 2016). In this perspective it is also significant that studies that describe the sensitivity of static and dynamic connectivity of channel deposits to channel-body characteristics fundamentally rely on object-based models (McKenna and Smith, 2004; de Jager et al., 2009; Larue and Friedmann, 2005; Larue and Hovadik, 2006; Hovadik and Larue, 2007; Burns et al., 2010; Jha et al., 2016; Peter et al., 2017). Understanding of how these parameters tend to co-vary, which has been overlooked in previous studies, can be used to obtain quantitative descriptions of common trends in the connectivity of channelized units, and to reduce the associated uncertainty.

Most object-based modeling algorithms have been developed for simulating any type of channelized architecture, be it that of aquifers hosted in subglacial channel deposits or of oil reservoirs composed of submarine-channel fills. Improvement in existing modeling tools might be realized by adapting them to specific geologic contexts. For channelized fluvial successions, more accurate reproduction of distributions and incorporation of observed scaling relationships in channel-body morphometry would likely result in a reduction in output variability and in more

realistic subsurface reconstructions. Although not discussed here, there are also other aspects of channelized fluvial architectures that are important and that object-based modeling tools should attempt to reproduce, such as autogenic channel-body clustering (cf. Villamizar et al., 2015), and channel-body splitting of tributary, distributary or avulsive nature (cf. Pyrcz et al., 2009).

Several other object-based modeling algorithms have been developed as proprietary, commercial or research-oriented software: results and considerations presented here cannot be generalized to these, as they have not been assessed.

7. Conclusions

Based on data from 61 analog studies, an empirical characterization of the geometry of fluvial channel bodies has been undertaken that describes distributions in, and relationships between, sandbody thickness, cross-stream width, and mean planform wavelength and amplitude. The data have been synthesized in empirical equations that can be used for constraining models of subsurface fluvial architecture, particularly when object-based models need to be built in data-poor situations.

The analog data have also been used to test the intrinsic realism of four object-based modeling algorithms, applied following nine different modeling approaches, by comparing characteristics of the modeled channelized architectures against fundamental patterns identified across the analogs.

Results from this assessment indicate aspects of each modeling approach that are not a good reflection of the geologic organization seen in the studied analogs. Although this type of information is not necessarily sufficient for establishing a best practice in building fluvial reservoir or aquifer models with object-based techniques, it is useful for raising awareness of pitfalls and limitations in the application of each modeling method. In particular, the choice of modeling strategy can be guided by the results presented here, in consideration of the characteristics of sedimentary architecture that are believed to be important for the case study at hand and that hence need to be honored.

Acknowledgements

Total E&P UK are thanked for funding this research. FRG-ERG sponsors (AkerBP, Areva, BHPBilliton, Cairn India [Vedanta], ConocoPhillips, Murphy Oil, Nexen Energy, Saudi Aramco, Shell, Tullow Oil, Woodside, and YPF) and our partner Petrotechnical Data Systems are thanked for financial support of the research group. LC has been supported by NERC (Catalyst Fund award NE/M007324/1; Follow-on Fund NE/N017218/1). We thank Schlumberger for providing academic licenses for Petrel. Associate Editor William Craddock, reviewer Kevin Keogh and an anonymous reviewer are thanked for their constructive criticism, which helped improve the article.

References cited

- Alexander, J., 1993, A discussion on the use of analogues for reservoir geology, *in* Ashton, M. (ed.) *Advances in Reservoir Geology*: Geological Society, London, Special Publication 69, p. 175-194, doi:10.1144/GSL.SP.1993.069.01.08.
- Alqahtani, F. A., H. D. Johnson, C. A.-L. Jackson, and M. R. B. Som, 2015, Nature, origin and evolution of a Late Pleistocene incised valley-fill, Sunda Shelf, Southeast Asia: *Sedimentology*, v. 62, p. 1198-1232, doi:10.1111/sed.12185.
- Berendsen, H. J. A., and E. Stouthamer, 2001, *Palaeogeographic development of the Rhine-Meuse delta, the Netherlands*: Assen, Koninklijke Van Gorcum, 268 p., doi:10.1046/j.1365-3091.2002.00469_1.x.
- Bezrukov, A., and A. R. Davletova, 2010, *Implementation Prospects Of Multi-Point Statistics Methods Into The Practice Of Geological Modeling*: Society of Petroleum Engineers, Russian Oil and Gas Conference and Exhibition, Moscow, Russia, SPE paper 135911, doi:10.2118/135911-MS.
- Biteman, S. E., D. W. Hyndman, M. S. Phanikumar, and G. S. Weissmann, 2004, Integration of Sedimentologic and Hydrogeologic Properties for Improved Transport Simulations, *in* Bridge, J. S., and D. W. Hyndman, eds., *Aquifer Characterization*: SEPM Special Publication 80, p. 3-13, doi:10.2110/pec.04.80.0003.

- Boucher, A., R. Gupta, J. Caers, and A. Satija, 2010, Tetris: a training image generator for SGeMS: Stanford Center for Reservoir Forecasting.
- Bridge, J. S., and M. R. Leeder, 1979, A simulation model of alluvial stratigraphy: *Sedimentology*, v. 26, p. 617-644, doi:10.1111/j.1365-3091.1979.tb00935.x
- Bridge, J. S., G. A. Jalfin, and S. M. Georgieff, 2000, Geometry, lithofacies, and spatial distribution of Cretaceous fluvial sandstone bodies, San Jorge Basin, Argentina: outcrop analog for the hydrocarbon-bearing Chubut Group: *Journal of Sedimentary Research*, v. 70, p. 341-359, doi:10.1306/2DC40915-0E47-11D7-8643000102C1865D.
- Burns, E. R., L. R. Bentley, M. Hayashi, S. E. Grasby, A. P. Hamblin, D. G. Smith, and P. R. Wozniak, 2010, Hydrogeological implications of paleo-fluvial architecture for the Paskapoo Formation, SW Alberta, Canada: a stochastic analysis: *Hydrogeology Journal*, v. 18, p. 1375-1390, doi:10.1007/s10040-010-0608-y.
- Clemetsen, R., A. R. Hurst, R. Knarud, and H. Omre, 1990, A computer program for evaluation of fluvial reservoirs, *in* Buller, A. T., E. Berg, O. Hjemeland, J. Kleppe, O. Torsaeter, and J. O. Aasen, eds., *North Sea oil and gas reservoirs II*: London, Graham and Trotman, p. 373-385, doi:10.1007/978-94-009-0791-1_32.
- Colombera, L., N. P. Mountney, and W. D. McCaffrey, 2012, A relational database for the digitization of fluvial architecture: concepts and example applications: *Petroleum Geoscience*, v. 18, p. 129-140, doi:10.1144/1354-079311-021.
- Colombera, L., N. P. Mountney, and W. D. McCaffrey, 2013, A quantitative approach to fluvial facies models: methods and example results: *Sedimentology*, v. 60, p. 1526-1558, doi:10.1111/sed.12050.
- Colombera, L., N. P. Mountney, F. Felletti, and W. D. McCaffrey, 2014, Models for guiding and ranking well-to-well correlations of channel bodies in fluvial reservoirs: *AAPG Bulletin*, v. 98, p. 1943-1965, doi:10.1306/05061413153.
- Colombera, L., N. P. Mountney, and W. D. McCaffrey, 2015, A meta-study of relationships between fluvial channel-body stacking pattern and aggradation rate: implications for sequence stratigraphy: *Geology*, v. 43, p. 283-286, doi:10.1130/G36385.1.

Colombera, L., N. P. Mountney, J. A. Howell, A. Rittersbacher, F. Felletti, and W. D. McCaffrey, 2016a, A test of analog-based tools for quantitative prediction of large-scale fluvial architecture: AAPG Bulletin, v. 100, p. 237-267, doi:10.1306/11181514227.

Colombera, L., M. N. Shiers, and N. P. Mountney, 2016b, Assessment of backwater controls on the architecture of distributary-channel fills in a tide-influenced coastal-plain succession: Campanian Neslen formation, USA: Journal of Sedimentary Research, v. 86, p. 476-497, doi:10.2110/jsr.2016.33.

Colombera, L., O. J. Arévalo, and N. P. Mountney, 2017, Fluvial-system response to climate change: The Paleocene-Eocene Tremp Group, Pyrenees, Spain: Global and Planetary Change, v. 157, p. 1-17, doi:10.1016/j.gloplacha.2017.08.011.

Dagan, G., 2002, An overview of stochastic modeling of groundwater flow and transport: From theory to applications: Eos, Transactions American Geophysical Union, v. 83, p. 621-625, doi:10.1029/2002EO000421.

Dalrymple, M., 2001, Fluvial reservoir architecture in the Statfjord Formation (northern North Sea) augmented by outcrop analogue statistics: Petroleum Geoscience, v. 7, p. 115-122, doi:10.1144/petgeo.7.2.115.

de Jager, G., J. F. Van Doren, J. D. Jansen, and S. M. Luthi, 2009, An evaluation of relevant geological parameters for predicting the flow behaviour of channelized reservoirs: Petroleum Geoscience, v. 15, p. 345-354, doi:10.1144/1354-079309-819.

de Marsily, G., F. Delay, J. Goncalves, P. Renard, V. Teles, and S. Violette, 2005, Dealing with spatial heterogeneity: Hydrogeology Journal, v. 13, p. 161-183, doi:10.1007/s10040-004-0432-3.

Deutsch, C. V., and T. T. Tran, 2002, FLUVSIM: a program for object-based stochastic modeling of fluvial depositional systems: Computers & Geosciences, v. 28, p. 525-535, doi:10.1016/S0098-3004(01)00075-9.

Eskandaridavand, K., and S. Srinivasan, 2010, Reservoir Modelling of Complex Geological Systems—A Multiple-Point Perspective: Journal of Canadian Petroleum Technology, v. 49, p. 59-69, doi:10.2118/139917-PA.

Fabuel-Perez, I., D. Hodgetts, and J. Redfern, 2010, Integration of digital outcrop models (DOMs) and high resolution sedimentology–workflow and implications for geological modelling: Oukaimeden Sandstone Formation, High Atlas (Morocco): *Petroleum Geoscience*, v. 16, p. 133-154, doi:10.1144/1354-079309-820.

Feyen, L., and J. Caers, 2006, Quantifying geological uncertainty for flow and transport modeling in multi-modal heterogeneous formations: *Advances in Water Resources*, v. 29, p. 912-929, doi:10.1016/j.advwatres.2005.08.002.

Fielding, C. R., and R. C. Crane, 1987, An application of statistical modelling to the prediction of hydrocarbon recovery factors in fluvial reservoir sequences, *in* Ethridge, F. G., R. M. Flores, and M. D. Harvey, eds., *Recent developments in fluvial sedimentology*: SEPM Special Publication 39, 321-327, doi:10.2110/pec.87.39.0321.

Fryirs, K. A., J. M. Wheaton, and G. J. Brierley, 2016, An approach for measuring confinement and assessing the influence of valley setting on river forms and processes: *Earth Surface Processes and Landforms*, v. 41, p. 701-710, doi:10.1002/esp.3893.

Giambastiani, B. M. S., A. M. McCallum, M. S. Andersen, B. F. J. Kelly, and R. I. Acworth, 2012, Understanding groundwater processes by representing aquifer heterogeneity in the Maules creek catchment, Namoi valley (New South Wales, Australia): *Hydrogeology Journal*, v. 20, p. 1027-1044, doi:10.1007/s10040-012-0866-y.

Gibling, M. R., 2006, Width and thickness of fluvial channel bodies and valley fills in the geological record: a literature compilation and classification: *Journal of Sedimentary Research*, v. 76, p. 731-770, doi:10.2110/jsr.2006.060.

Gottschalk, I. P., T. Hermans, R. Knight, J. Caers, D. A. Cameron, J. Regnery, and J. E. McCray, 2017, Integrating Non-Colocated Well and Geophysical Data to Capture Subsurface Heterogeneity at an Aquifer Recharge and Recovery Site: *Journal of Hydrology*, v. 555, p. 407-419, doi:10.1016/j.jhydrol.2017.10.028.

Guardiano, F. B., and R. M. Srivastava, 1993, Multivariate geostatistics: beyond bivariate moments, *in* Soares, A., ed., *Geostatistics Troia '92* v. 1: Dordrecht, Kluwer Academic, p. 133-144, doi:10.1007/978-94-011-1739-5_12.

Gundesø, R., and O. Egeland, 1990, SESIMIRA—a new geological tool for 3D modelling of heterogeneous reservoirs, *in* Buller, A. T., E. Berg, O. Hjemeland, J. Kleppe, O. Torsaeter, and J. O. Aasen, eds., North Sea oil and gas reservoirs II: London, Graham and Trotman, p. 363-371, doi:10.1007/978-94-009-0791-1_31.

Hirst, J. P. P., C. R. Blackstock, and S. Tyson, 1993, Stochastic modelling of fluvial sandstone bodies, *in* Flint, S., and I. D. Bryant, eds., The Geological Modelling of Hydrocarbon Reservoirs and Outcrop Analogues: International Association of Sedimentologists Special Publication 15, p. 237-251, doi:10.1002/9781444303957.ch15.

Holden, L., R. Hauge, Ø. Skare, and A. Skorstad, 1998, Modeling of fluvial reservoirs with object models: *Mathematical Geology*, v. 30, p. 473-496, doi:10.1023/A:1021769526425.

Hovadik, J. M., and D. K. Larue, 2007, Static characterizations of reservoirs: refining the concepts of connectivity and continuity: *Petroleum Geoscience*, v. 13, p. 195-211, doi:10.1144/1354-079305-697.

Howell, J. A., A. W. Martinius, and T. R. Good, 2014, The application of outcrop analogues in geological modelling: A review, present status and future outlook, *in* Martinius, A. W., J. A. Howell, and T. R. Good, eds., Sediment-Body Geometry and Heterogeneity: Analogue Studies for Modelling the Subsurface: Geological Society, London, Special Publication 387, p. 1-25, doi:10.1144/SP387.12.

Höyng, D., F. M. D’Affonseca, P. Bayer, E. G. de Oliveira, J. A. J. Perinotto, F. Reis, H. Weiss, and P. Grathwohl, 2014, High-resolution aquifer analog of fluvial–aeolian sediments of the Guarani aquifer system: *Environmental Earth Sciences*, v. 71, p. 3081-3094, doi:10.1007/s12665-013-2684-5.

Issautier, B., S. Viseur, P. Audigane, and Y. M. Le Nindre, 2014, Impacts of fluvial reservoir heterogeneity on connectivity: implications in estimating geological storage capacity for CO₂: *International Journal of Greenhouse Gas Control*, v. 20, p. 333-349, doi:10.1016/j.ijggc.2013.11.009.

Jeong, H., and S. Srinivasan, 2016, Fast assessment of CO₂ plume characteristics using a connectivity based proxy: *International Journal of Greenhouse Gas Control*, v. 49, p. 387-412, doi:10.1016/j.ijggc.2016.03.001.

Jha, S. K., G. Mariethoz, G. Mathews, J. Vial, and B. F. Kelly, 2016, Influence of Alluvial Morphology on Upscaled Hydraulic Conductivity: *Groundwater*, v. 54, p. 384-393, doi:10.1111/gwat.12378.

Jordan, D. W., and W. A. Pryor, 1992, Hierarchical levels of heterogeneity in a Mississippi River meander belt and application to reservoir systems: *AAPG Bulletin*, v. 76, p. 1601-1624.

Keogh, K. J., A. W. Martinius, and R. Osland, 2007, The development of fluvial stochastic modelling in the Norwegian oil industry: A historical review, subsurface implementation and future directions: *Sedimentary Geology*, v. 202, p. 249-268, doi: 10.1016/j.sedgeo.2007.05.009.

Kerrou, J., P. Renard, H. J. H. Franssen, and I. Lunati, 2008, Issues in characterizing heterogeneity and connectivity in non-multiGaussian media: *Advances in Water Resources*, v. 31, p. 147-159, doi:10.1016/j.advwatres.2007.07.002.

Kjemperud, A. V., E. R. Schomacker, and T. A. Cross, 2008, Architecture and stratigraphy of alluvial deposits, Morrison Formation (Upper Jurassic), Utah: *AAPG Bulletin*, v. 92, p. 1055-1076, doi:10.1306/03250807115.

Klise, K. A., G. S. Weissmann, S. A. McKenna, E. M. Nichols, J. D. Frechette, T. F. Wawrzyniec, and V. C. Tidwell, 2009, Exploring solute transport and streamline connectivity using lidar-based outcrop images and geostatistical representations of heterogeneity: *Water Resources Research*, v. 45, W05413, doi:10.1029/2008WR007500

Labourdette, R., 2011, Stratigraphy and static connectivity of braided fluvial deposits of the lower Escanilla Formation, south central Pyrenees, Spain: *AAPG Bulletin*, v. 95, p. 585-617, doi:10.1306/08181009203.

Labourdette, R., and R. R. Jones, 2007, Characterization of fluvial architectural elements using a three-dimensional outcrop data set: Escanilla braided system, South-Central Pyrenees, Spain: *Geosphere*, v. 3, p. 422-434, doi:10.1130/GES00087.1.

Larriestra, C. N., and H. Gomez, 2010, Multiple-point simulation applied to uncertainty analysis of reservoirs related to high sinuosity fluvial systems: *Mina El*

Carmen Formation, San Jorge Gulf Basin, Argentina: AAPG Search and Discovery, article 40515.

Larue, D. K., and F. Friedmann, 2005, The controversy concerning stratigraphic architecture of channelized reservoirs and recovery by waterflooding: *Petroleum Geoscience*, v. 11, p. 131-146, doi:10.1144/1354-079304-626.

Larue, D. K., and J. Hovadik, 2006, Connectivity of channelized reservoirs: a modelling approach: *Petroleum Geoscience*, v. 12, p. 291-308, doi:10.1144/1354-079306-699.

Leopold, L. B., and M. G. Wolman, 1960, River meanders: *Geological Society of America Bulletin*, v. 71, p. 769-793, doi:10.1130/0016-7606(1960)71[769:RM]2.0.CO;2

Liu, Y., and S. Atan, 2008, A study of static modeling factors that are critical to flow simulation: *International Petroleum Technology Conference*, Kuala Lumpur, Malaysia, IPTC paper 12894, doi:10.2523/IPTC-12894-MS.

Maharaja, A., 2008, TiGenerator: object-based training image generator: *Computers & Geosciences*, v. 34, p. 1753-1761, doi:10.1016/j.cageo.2007.08.012.

Marini, M., Felletti, F., Beretta, G. P., and Terrenghi, J., 2018, Three geostatistical methods for hydrofacies simulation ranked using a large borehole lithology dataset from the Venice hinterland (NE Italy): *Water*, v. 10, 844, doi:10.3390/w10070844.

Maynard, K., and I. Murray, 2003, One million years from the Upper Arang Formation, West Natuna Basin, implications for reservoir distribution and facies variation in fluvial deltaic deposits: *Indonesian Petroleum Association, 29th Annual Convention Proceedings*, v. 1, p. 270-276.

McKenna, S. A., and G. Smith, 2004, Sensitivity of groundwater flow patterns to parameterization of object-based fluvial aquifer models, in Bridge, J. S., and D. W. Hyndman, eds., *Aquifer Characterization: SEPM Special Publication 80*, p. 29-40, doi:10.2110/pec.04.80.0029.

McNally, G. H., and I. R. Wilson, 1996, Silcretes of the Mirackina Palaeochannel, Arckaringa, South Australia: *AGSO Journal of Australian Geology and Geophysics*, v. 16, p. 295-301.

Miall, A. D., 1985, Architectural-element analysis: A new method of facies analysis applied to fluvial deposits: *Earth-Science Reviews*, v. 22, p. 261-308, doi:10.1016/0012-8252(85)90001-7.

Nguyen, M. C., X. Zhang, N. Wei, J. Li, X. Li, Y. Zhang, and P. H. Stauffer, 2017, An object-based modeling and sensitivity analysis study in support of CO₂ storage in deep saline aquifers at the Shenhua site, Ordos Basin: *Geomechanics and Geophysics for Geo-Energy and Geo-Resources*, v. 3, p. 293-314, doi: 10.1007/s40948-017-0063-5.

Norden, B., and P. Frykman, 2013, Geological modelling of the Triassic Stuttgart Formation at the Ketzin CO₂ storage site, Germany: *International Journal of Greenhouse Gas Control*, v. 19, p. 756-774, doi:10.1016/j.ijggc.2013.04.019.

Peter, C., Q. Sacchi, C. Serazio, and F. Verga, 2017, Capturing channelized reservoir connectivity uncertainty with amalgamation curves: *Marine and Petroleum Geology*, v. 88, p. 329-342, doi:10.1016/j.marpetgeo.2017.07.017.

Pirot, G., P., Renard, E., Huber, J., Straubhaar, and P. Huguenberger, 2015, Influence of conceptual model uncertainty on contaminant transport forecasting in braided river aquifers: *Journal of Hydrology*, v. 531, p. 124-141, doi:10.1016/j.jhydrol.2015.07.036.

Pranter, M. J., A. I. Ellison, R. D. Cole, and P. E. Patterson, 2007, Analysis and modeling of intermediate-scale reservoir heterogeneity based on a fluvial point-bar outcrop analog, Williams Fork Formation, Piceance Basin, Colorado: *AAPG Bulletin*, v. 91, p. 1025-1051, doi:10.1306/02010706102.

Pranter, M. J., A. C. Hewlett, R. D. Cole, H. Wang, and J. Gilman, 2014, Fluvial architecture and connectivity of the Williams Fork Formation: use of outcrop analogues for stratigraphic characterization and reservoir modelling, *in* Martinius, A. W., J. A. Howell, and T. R. Good, eds., *Sediment-Body Geometry and Heterogeneity: Analogue Studies for Modelling the Subsurface*: Geological Society, London, Special Publication 387, p. 57-83, doi:10.1144/SP387.1.

Pyrzcz, M. J., J. B. Boisvert, and C. V. Deutsch, 2008, A library of training images for fluvial and deepwater reservoirs and associated code: *Computers & Geosciences*, v. 34, p. 542-560, doi:10.1016/j.cageo.2007.05.015.

- Pyrzcz, M. J., J. B. Boisvert, and C. V. Deutsch, 2009, ALLUVSIM: A program for event-based stochastic modeling of fluvial depositional systems. *Computers & Geosciences*, v. 35, p. 1671-1685, doi:10.1016/j.cageo.2008.09.012.
- Reynolds, A. D., 1999, Dimensions of paralic sandstone bodies: *AAPG Bulletin*, v. 83, p. 211-229, doi:10.1306/00AA9A48-1730-11D7-8645000102C1865D.
- Ringrose, P., and M. Bentley, 2015, *Reservoir Model Design – A Practitioner’s Guide*: Berlin, Springer, 249 p., doi:10.1007/978-94-007-5497-3.
- Rittersbacher, A., J. A. Howell, and S. J. Buckley, 2014, Analysis of fluvial architecture in the Blackhawk Formation, Wasatch Plateau, Utah, USA, using large 3D photorealistic models: *Journal of Sedimentary Research*, v. 84, p. 72-87, doi:10.2110/jsr.2014.12.
- Robinson, J. W., and P. J. McCabe, 1997, Sandstone-body and shale-body dimensions in a braided fluvial system: Salt Wash Sandstone Member (Morrison Formation), Garfield County, Utah: *AAPG Bulletin*, v. 81, p. 1267-1291.
- Rojas, T. S., 2013, Controlling realism and uncertainty in reservoir models using intelligent sedimentological prior information, PhD thesis, Heriot-Watt University, Edinburgh, 264 p.
- Ronayne, M. J., S. M. Gorelick, and J. Caers, 2008, Identifying discrete geologic structures that produce anomalous hydraulic response: An inverse modeling approach: *Water Resources Research*, v. 44, W08426, doi:10.1029/2007WR006635.
- Rubin, Y., I. A. Lunt, and J. S. Bridge, 2006, Spatial variability in river sediments and its link with river channel geometry: *Water Resources Research*, v. 42, W06D16, doi:10.1029/2005WR004853.
- Schneider, C. A., W. S. Rasband, and K. W. Eliceiri, 2012, NIH Image to ImageJ: 25 years of image analysis: *Nature Methods*, v. 9, p. 671-675, doi:10.1038/nmeth.2089.
- Stølum, H. H., 1998, Planform geometry and dynamics of meandering rivers. *Geological Society of America Bulletin*, 110, 1485-1498, doi:10.1130/0016-7606(1998)110<1485:PGADOM>2.3.CO;2.

Strebelle, S., 2002, Conditional simulation of complex geological structures using multiple-point statistics: *Mathematical Geology*, v. 34, p. 1-21, doi:10.1023/A:1014009426274.

Villamizar, C. A., G. J. Hampson, Y. S. Flood, and P. J. Fitch, 2015, Object-based modelling of avulsion-generated sandbody distributions and connectivity in a fluvial reservoir analogue of low to moderate net-to-gross ratio: *Petroleum Geoscience*, v. 21, p. 249-270, doi:10.1144/petgeo2015-004.

Viseur, S., A. Shtuka, and J. L. Mallet, 1998, New Fast, Stochastic, Boolean Simulation of Fluvial Deposits: Society of Petroleum Engineers, Annual Technical Conference and Exhibition, New Orleans, USA, SPE paper 49281, doi:10.2118/49281-MS

Willems, C. J., H. M. Nick, M. E. Donselaar, G. J. Weltje, and D. F. Bruhn, 2017, On the connectivity anisotropy in fluvial Hot Sedimentary Aquifers and its influence on geothermal doublet performance: *Geothermics*, v. 65, p. 222-233, doi:10.1016/j.geothermics.2016.10.002.

Williams, G. P., 1986, River meanders and channel size: *Journal of Hydrology*, v. 88, p. 147-164, doi:10.1016/0022-1694(86)90202-7.

Williams, R. M., T. C. Chidsey Jr, and D. E. Eby, 2007, Exhumed paleochannels in central Utah—Analogues for raised curvilinear features on Mars, *in* Willis, G. C., M. D. Hylland, D. L. Clark, and T. C. Chidsey Jr., eds., *Central Utah—Diverse Geology of a Dynamic Landscape*: Utah Geological Association Publication 36, 221-235.

Zovi, F., M. Camporese, H. J. H. Franssen, J. A. Huisman, and P. Salandin, 2017, Identification of high-permeability subsurface structures with multiple point geostatistics and normal score ensemble Kalman filter: *Journal of Hydrology*, v. 548, p. 208-224, doi:10.1016/j.jhydrol.2017.02.056.

SUPPLEMENTARY MATERIAL**List of published sources that contain data used in this work.**

Alqahtani F. A., Jackson C. A.-L., Johnson H. D., Som M. R. B. (2017) Controls on the geometry and evolution of humid-tropical fluvial systems: insights from 3D seismic geomorphological analysis of the Malay Basin, Sunda Shelf, Southeast Asia. *J. Sed. Res.* 87, 17-40.

Alqahtani F. A., Johnson H. D., Jackson C. A.-L., Som M. R. B. (2015) Nature, origin and evolution of a Late Pleistocene incised valley-fill, Sunda Shelf, Southeast Asia. *Sedimentology* 62, 1198-1232.

Amorosi A., Pavesi M., Ricci Lucchi M., Sarti G., Piccin A. (2008) Climatic signature of cyclic fluvial architecture from the Quaternary of the central Po Plain, Italy. *Sed. Geol.* 209, 58-68.

Berendsen H. J. A., Stouthamer E. (2001) Palaeogeographic Development of the Rhine–Meuse Delta, The Netherlands. Koninklijke Van Gorcum, 268 pp.

Bridge J. S., Jalfin G. A., Georgieff S. M. (2000) Geometry, lithofacies, and spatial distribution of Cretaceous fluvial sandstone bodies, San Jorge Basin, Argentina: outcrop analog for the hydrocarbon-bearing Chubut Group. *J. Sed. Res.* 70, 341-359.

Carter D. C. (2003) 3-D seismic geomorphology: insights into fluvial reservoir deposition and performance, Widuri field, Java Sea. *AAPG Bull.* 87, 909-934.

Cuevas Martínez J. L., Cabrera Perez L., Marcuello A., Arbues Cazo P., Marzo Carpio M., Bellmunt F. (2010) Exhumed channel sandstone networks within fluvial fan deposits from the Oligo-Miocene Caspe Formation, South-east Ebro Basin (North-east Spain). *Sedimentology* 57, 162-189.

Dalrymple M. (2001) Fluvial reservoir architecture in the Staffjord Formation (northern North Sea) augmented by outcrop analogue statistics. *Pet. Geosc.*, 7, 115-122.

Darmadi Y., Willis B. J., Dorobek S. L. (2007) Three-dimensional seismic architecture of fluvial sequences on the low-gradient Sunda Shelf, offshore Indonesia. *J. Sed. Res.* 77, 225-238.

Donselaar M. E., Overeem I. (2008) Connectivity of fluvial point-bar deposits: An example from the Miocene Huesca fluvial fan, Ebro Basin, Spain. *AAPG Bull.* 92, 1109-1129.

Dreyer T. (1993) Quantified fluvial architecture in ephemeral stream deposits of the Esplugafreda Formation (Palaeocene), Tremp-Graus basin, northern Spain. In: Marzo M., Puidefábregas C. (Eds.) *Alluvial sedimentation*, IAS Spec. Publ. 17, 337-362.

Erhardt A. M. (2005) Relative contributions of tectonics and climate on fluvial sedimentation in the Wasatch Formation of Western Colorado. Unpublished MSc Thesis, Colorado School of Mines, Golden, USA.

Fachmi M., Wood L. J. (2005) Seismic geomorphology: a study from West Natuna Basin, Indonesia. *Indonesian Petroleum Association 30th Annual Convention Proceedings*, vol. 1, 163-178.

Fielding C. R. (1986) Fluvial channel and overbank deposits from the Westphalian of the Durham coalfield, NE England. *Sedimentology* 33, 119-140.

Fielding C. R., Crane R. C. (1987) An application of statistical modelling to the prediction of hydrocarbon recovery factors in fluvial reservoir sequences. In: Ethridge F. G., Flores R. M., Harvey M. D. (eds.) *Recent Developments in Fluvial Sedimentology*. SEPM Spec. Publ. 39, 321-327.

Flores R. M., Stricker G. D. (1993) Early Cenozoic depositional systems, Wishbone Hill District, Matanuska coal field, Alaska. In: Dusel-Bacon C., Till A. B. (eds.) *Geologic Studies in Alaska by the Geological Survey, 1992*. USGS Bull. 2068, 101-117.

Ford G. L., Pyles D. R. (2014) A hierarchical approach for evaluating fluvial systems: Architectural analysis and sequential evolution of the high net-sand content middle Wasatch Formation, Uinta Basin, Utah. *AAPG Bull.* 98, 1273-1304.

Foreman B. Z. (2014) Climate-driven generation of a fluvial sheet sand body at the Paleocene–Eocene boundary in north-west Wyoming (USA). *Basin Res.* 26, 225-241.

Foreman B. Z., Heller P. L., Clementz M. T. (2012) Fluvial response to abrupt global warming at the Palaeocene/Eocene boundary. *Nature* 491, 92-95.

Friend P. F., Raza S. M., Geehan G., Sheikh K. A. (2001) Intra- and extrabasinal controls on fluvial deposition in the Miocene Indo-Gangetic foreland basin, northern Pakistan. *J. Geol. Soc.* 158, 163-177.

Gouw M. J. (2008). Alluvial architecture of the Holocene Rhine–Meuse delta (the Netherlands). *Sedimentology* 55, 1487-1516.

Gouw M. J., Berendsen H. J. A. (2007). Variability of channel-belt dimensions and the consequences for alluvial architecture: observations from the Holocene Rhine–Meuse Delta (the Netherlands) and Lower Mississippi Valley (USA). *Journal of Sedimentary Research*, 77(2), 124-138.

Hajek E. A., Heller P. L., Sheets B. A. (2010) Significance of channel-belt clustering in alluvial basins. *Geology* 38, 535-538.

Hampson G. J., Gani M. R., Sahoo H., Rittersbacher A., Irfan N., Ranson A., Jewell T. O., Gani N. D. S., Howell J. A., Buckley S. J., Bracken B. (2012) Controls on large-scale patterns of fluvial sandbody distribution in alluvial to coastal plain strata: Upper Cretaceous Blackhawk Formation, Wasatch Plateau, Central Utah, USA. *Sedimentology* 59, 2226-2258.

Hirst J. P. P. (1991) Variations in alluvial architecture across the Oligo-Miocene Huesca fluvial system, Ebro Basin, Spain. In: Miall A. D., Tyler N. (eds.) *The three-dimensional facies architecture of terrigenous clastic sediments and its implications for hydrocarbon discovery and recovery*. SEPM Concepts in Sed. and Paleo. 3, 111-121.

Jo H. R. (2003) Depositional environments, architecture, and controls of Early Cretaceous non-marine successions in the northwestern part of Kyongsang Basin, Korea. *Sed. Geol.* 161, 269-294.

- Jordan D. W., Pryor W. A. (1992) Hierarchical levels of heterogeneity in a Mississippi River meander belt and application to reservoir systems. AAPG Bull. 76, 1601-1624.
- Keighley D., Flint S., Howell J., Moscariello A. (2003) Sequence stratigraphy in lacustrine basins: a model for part of the Green River Formation (Eocene), southwest Uinta Basin, Utah, USA. J. Sed. Res. 73, 987-1006.
- Kjemperud A. V., Schomacker E. R., Cross T. A. (2008) Architecture and stratigraphy of alluvial deposits, Morrison Formation (Upper Jurassic), Utah. AAPG Bull. 92, 1055-1076.
- Kraus M. J. (1996) Avulsion deposits in lower Eocene alluvial rocks, Bighorn Basin, Wyoming. J. Sed. Res. 66, 354-363.
- Kraus M. J., Aslan A. (1993) Eocene hydromorphic paleosols: significance for interpreting ancient floodplain processes. J. Sed. Petr. 63, 453-463.
- Kraus M. J., Davies-Vollum K. S. (2004) Mudrock-dominated fills formed in avulsion splay channels: examples from the Willwood Formation, Wyoming. Sedimentology 51, 1127-1144.
- Kraus M. J., Gwinn B. (1997) Facies and facies architecture of paleogene floodplain deposits, Willwood formation, Bighorn Basin, Wyoming, USA. Sed. Geol. 114, 33-54.
- Labourdette R. (2011) Stratigraphy and static connectivity of braided fluvial deposits of the lower Escanilla Formation, south central Pyrenees, Spain. AAPG Bull. 95, 585-617.
- Makaske B., Berendsen H. J. A., van Ree M. H. M. (2007) Middle Holocene Avulsion-Belt Deposits in the Central Rhine–Meuse Delta, The Netherlands. J. Sed. Res. 77, 110-123.
- Martinius A. W., Nieuwenhuijs R. A. (1995) Geological description of flow units in channel sandstones in a fluvial reservoir analogue (Loranca Basin, Spain). Pet. Geosc. 1, 237-252.
- Maynard J. R. (2006) Fluvial response to active extension: evidence from 3D seismic data from the Frio Formation (Oligo-Miocene) of the Texas Gulf of Mexico Coast, USA. Sedimentology 53, 515-536.
- Maynard J. R., Feldman H. R., Alway R. (2010) From bars to valleys: the sedimentology and seismic geomorphology of fluvial to estuarine incised-valley fills of the Grand Rapids Formation (Lower Cretaceous), Iron River Field, Alberta, Canada. J. Sed. Res. 80, 611-638.
- Maynard K., Murray I. (2003) One million years from the Upper Arang Formation, West Natuna Basin, implications for reservoir distribution and facies variation in fluvial deltaic deposits. Indonesian Petroleum Association 29th Annual Convention Proceedings, vol. 1, 270-276.
- Maynard K., Siregar P., Andria L. (2002) Seismic stratigraphic interpretation of a major 3-D, the Gabus sub-basin, blocks B and Tobong, West Natuna Sea, Indonesia: getting the geology back into seismic. Indonesian Petroleum Association 28th Annual Convention Proceedings, vol. 1, 87-104.

- McRae L. E. (1990) Paleomagnetic isochrons, unsteadiness, and non-uniformity of sedimentation in Miocene fluvial strata of the Siwalik Group, Northern Pakistan. *Jour. Geol.* 98, 433-456.
- Meadows N. S. (2006) The correlation and sequence architecture of the Ormskirk Sandstone Formation in the Triassic Sherwood Sandstone Group of the East Irish Sea Basin, NW England. *Geol. J.* 41, 93-122.
- Miall A. D. (2002) Architecture and sequence stratigraphy of Pleistocene fluvial systems in the Malay Basin, based on seismic time-slice analysis. *AAPG Bull.* 86, 1201-1216.
- Mohrig D., Heller P. L., Paola C., Lyons, W. J. (2000) Interpreting avulsion process from ancient alluvial sequences: Guadalupe-Matarranya system (northern Spain) and Wasatch Formation (western Colorado). *Geol. Soc. Am. Bull.* 112, 1787-1803.
- Nádor A., Zstanó O. (2011) Lateral and vertical variability of channel belt stacking density as a function of subsidence and sediment supply: field evidence from the intramontaine Körös Basin, Hungary. In: Davidson S. K., Leleu S., North C. P. (eds.) *From river to rock record: the preservation of fluvial sediments and their subsequent interpretation.* SEPM Spec. Publ. 97, 375-392.
- North C. P., Taylor K. S. (1996) Ephemeral-fluvial deposits: integrated outcrop and simulation studies reveal complexity. *AAPG Bull.* 80, 811-830.
- Olsen T. (1995) Fluvial and fluvio-lacustrine facies and depositional environments of the Maastrichtian to Paleocene North Horn Formation, Price Canyon, Utah. *Mt. Geol.* 32, 27-44.
- Olsen T. (1995) Sequence stratigraphy, alluvial architecture and potential reservoir heterogeneities of fluvial deposits: evidence from outcrop studies in Price Canyon, Utah (Upper Cretaceous and Lower Tertiary). In: Steel R. J., Felt V. L., Johannessen E. P., Mathieu C. (eds.) *Sequence Stratigraphy on the Northwest European Margin.* NPF Spec. Publ. 5, 75-96.
- Paredes J. M., Foix N., Colombo Piñol F., Nillni A., Allard J. O., Marquillas R. A. (2007) Volcanic and climatic controls on fluvial style in a high-energy system: the Lower Cretaceous Matasiete Formation, Golfo San Jorge basin, Argentina. *Sed. Geol.* 202, 96-123.
- Rasmussen A. M. S. (2005) Reservoir characterization of a fluvial sandstone: depositional environment and heterogeneities in modeling of the Colton Formation, Utah. Unpublished MSc Thesis, University of Oslo, Norway.
- Reijenstein H.M., Posamentier H.W., Bhattacharya J.P. (2011) Seismic geomorphology and high-resolution seismic stratigraphy of inner-shelf fluvial, estuarine, deltaic, and marine sequences, Gulf of Thailand. *AAPG Bull.* 95, 1959-1990.
- Reynolds A. D. (1999) Dimensions of paralic sandstone bodies. *AAPG Bull.* 83, 211-229.
- Roberts E. M. (2007) Facies architecture and depositional environments of the Upper Cretaceous Kaiparowits Formation, southern Utah. *Sed. Geol.* 197, 207-233.

Roberts S. B. (1998) An overview of the stratigraphic and sedimentologic characteristics of the Paleocene Fort Union Formation, southern Bighorn Basin, Wyoming. In: Keefer W. R. & Goolsby J. E. (eds.) Cretaceous and lower Tertiary rocks of the Bighorn Basin, Wyoming and Montana. Wy. Geol. Ass. Guidebook 49, 91-116.

Robinson J. W., McCabe P. J. (1997) Sandstone-body and shale-body dimensions in a braided fluvial system: Salt Wash Sandstone Member (Morrison Formation), Garfield County, Utah. AAPG Bull. 81, 1267-1291.

Rogers R. R. (1998) Sequence analysis of the Upper Cretaceous Two Medicine and Judith River formations, Montana: nonmarine response to the Claggett and Bearpaw marine cycles. J. Sed. Res. 68, 615-631.

Rygel M. C., Gibling M. R. (2006) Natural geomorphic variability recorded in a high-accommodation setting: fluvial architecture of the Pennsylvanian Joggins Formation of Atlantic Canada. J. Sed. Res. 76, 1230-1251.

Samorn H. (2006) Fluvial reservoir architecture from near-surface 3D seismic data, Block B8/32, Gulf of Thailand. Unpublished MSc thesis, Colorado School of Mines, Golden, USA.

Additional data were derived from outcrop studies. Publications that contain the same datasets are reported below.

Colombera L., Mounney N. P., Howell J. A., Rittersbacher A., Felletti F., McCaffrey W. D. (2016) A test of analog-based tools for quantitative prediction of large-scale fluvial architecture. AAPG Bull. 100, 237-267.

Colombera L., Arévalo O. J., Mounney N. P. (2017) Fluvial-system response to climate change: The Paleocene-Eocene Tremp Group, Pyrenees, Spain. Glo. Pla. Cha. 157, 1-17.